Adv Polym Sci (2005) 182: 1–54
DOI 10.1007/b135559

Published online: 9 August 2005

Fractionation of Semicrystalline Polymers by Crystallization Analysis Fractionation and Temperature Rising Elution Fractionation

Siripon Anantawaraskul[1,3] · João B. P. Soares[2] (✉) · Paula M. Wood-Adams[4]

[1]Department of Chemical Engineering, McGill University, 3610 University Street, Montreal, H3A 2B2, Canada

[2]Department of Chemical Engineering, University of Waterloo, Waterloo, ON, N2L 3G1, Canada
jsoares@cape.uwaterloo.ca

[3]Department of Chemical Engineering, Kasetsart University, 50 Phaholyothin Road, 10900 Bangkok, Thailand

[4]Department of Mechanical and Industrial Engineering, Concordia University, 1455 de Maisonneuve Blvd. West, Montreal, H3G 1M8, Canada

Abstract Crystallization analysis fractionation (Crystaf) and temperature rising elution fractionation (Tref) are analytical techniques for determining the distribution of chain crystallizabilities of semicrystalline polymers. These techniques fractionate polymer chains on the basis of the differences in their chain microstructures that affect their crystallizabilities in dilute solutions. Both techniques can be used to estimate the chemical composition distribution of copolymers and the tacticity distribution of homopolymers. This information is crucial for understanding polymerization mechanisms and constructing structure–property relationships. This review covers the theoretical aspects of both techniques, describes their basic operation procedures and applications, and discusses the mathematical models proposed for Crystaf and Tref.

Keywords Chemical composition distribution · Composition heterogeneity · Crystallization analysis fractionation · Polyethylene · Polyolefins · Temperature rising elution fractionation

Abbreviations

A-Tref	Analytical temperature rising elution fractionation
CC	Average comonomer content
CCD	Chemical composition distribution
CR	Cooling rate
Crystaf	Crystallization analysis fractionation
DSC	Differential scanning calorimetry
FTIR	Fourier transform IR
HDPE	High-density polyethylene
LDPE	Low-density polyethylene
LLDPE	Linear low-density polyethylene
MWD	Molecular weight distribution
P-Tref	Preparative temperature rising elution fractionation
SEC	Size-exclusion chromatography
SNA	Successive nucleation/annealing
SSF	Successive solution fractionation
Tref	Temperature rising elution fractionation
ΔT_C	Temperature difference between Crystaf peak temperatures

1 Introduction

Polymer microstructural characterization provides information that is essential to understand polymerization mechanisms and to construct structure–property relationships required for the production of polymers with a set of well-defined molecular and macroscopic properties.

Crystallization analysis fractionation (Crystaf) is a recently developed characterization technique that fractionates polymer chains according to their crystallizabilities in a dilute solution [1, 2]. This technique is based on the continuous nonisothermal crystallization of polymer chains from a dilute solution. During crystallization, the concentration of polymer in solution is measured as a function of crystallization temperature, generating a cumulative concentration profile such as the one shown in Fig. 1. The derivative of this cumulative concentration profile is proportional to the fraction of polymer crystallized at each temperature interval and represents the distribution of chain crystallizabilities in the sample.

For ethylene/1-olefin copolymers, chain crystallizability is mainly controlled by the fraction of noncrystallizable comonomer units in the chain. Consequently, the differential Crystaf profile shown in Fig. 1, together with an appropriate calibration curve, can be used to estimate the copolymer chemical composition distribution (CCD), also called the short-chain branch distribution. The CCD of a copolymer describes the distribution of the

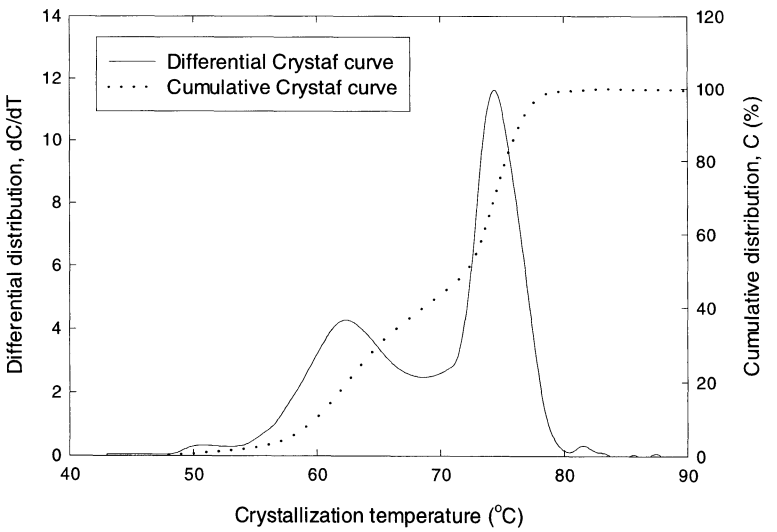

Fig. 1 Cumulative and differential crystallization analysis fractionation (*Crystaf*) profiles of a blend of two polyolefins

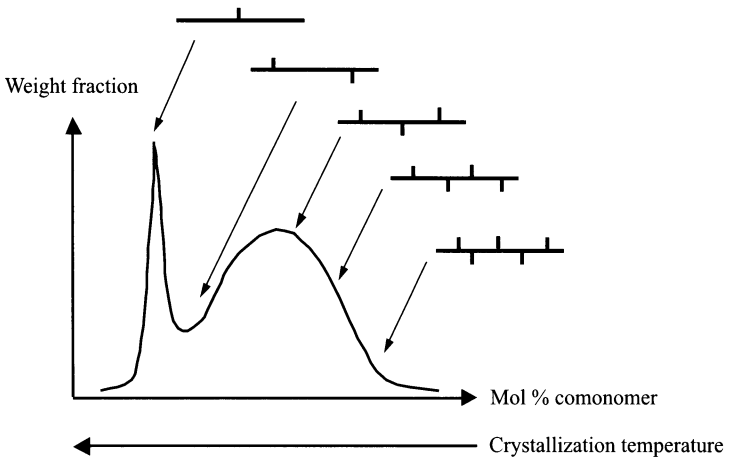

Fig. 2 Chemical composition distribution (*CCD*) of a typical Ziegler–Natta linear low-density polyethylene, reflecting the composition heterogeneity of these copolymers

comonomer fraction in its chains, reflecting its composition heterogeneity (Fig. 2). Composition heterogeneity in copolymers can significantly influence their physical properties. For example, linear low-density polyethylene (LLDPE) with a narrow CCD has much better film properties than LLDPE with a broad CCD [3, 4].

Several factors may contribute to CCD heterogeneity [5]. The more pervasive one is the statistical nature of polymerization which forces the composition of any synthetic copolymer chain to be always distributed around a certain average value. For multi-site-type catalysts, e.g. heterogeneous Ziegler–Natta catalysts, each active site type has a distinct set of polymerization kinetics constants and produces polymer chains with different average microstructures. Therefore, the polymers synthesized with these catalysts are mixtures of chains with different average chain lengths and average comonomer compositions (Fig. 3). Nonuniform polymerization conditions, i.e. temporal and spatial variations in monomer concentration and temperature during polymerization, may also be responsible for CCD heterogeneity. Comonomer compositional drift, a commonly encountered phenomenon in batch and semibatch polymerizations, can significantly broaden the CCD of copolymers.

In the case of stereoregular polymers, such as isotactic and syndiotactic polypropylene, chain tacticity is the main factor affecting crystallizability. Crystaf can also be used to measure the distribution of tacticity. Since the distribution of tacticity is often modeled with pseudo binary copolymerization models (i.e. the meso and racemic insertions stand for the comonomer type in the case of a copolymer), the following discussion for copolymers can be easily modified to describe the tacticity distribution of stereoregular polymers.

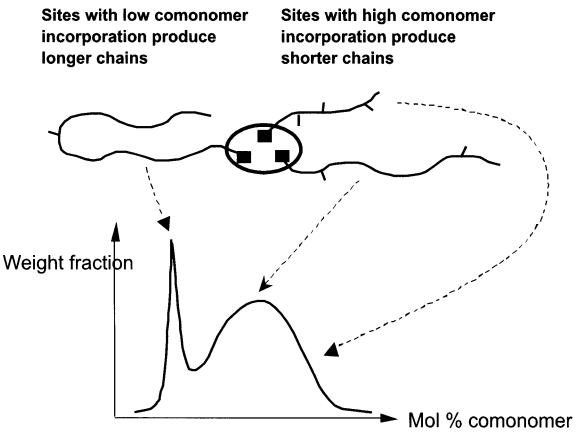

Fig. 3 Copolymers produced by Ziegler–Natta catalysts exhibiting a broad CCD. Chains made by different active sites have different microstructural distributions

Crystaf was developed as an alternative to temperature rising elution fractionation (Tref). Although both techniques are based on similar fractionation mechanisms and provide comparable results, Tref operation tends to be more time-consuming because it involves two fractionation steps, crystallization and elution, while Crystaf requires only the crystallization step. Similarly to Crystaf, the most important fractionation step in Tref occurs during the crystallization step, but data collection in Tref is done only during the elu-

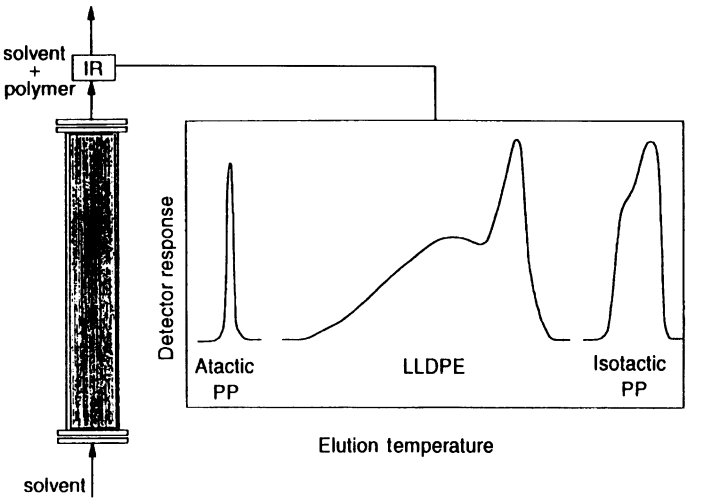

Fig. 4 Elution step of temperature rising elution fractionation (*Tref*) analysis and typical Tref profiles of different polymers [5]. *LLDPE* linear low-density polyethylene, *PP* polypropylene

tion period (Fig. 4). In this review, an overview of Tref operation will also be given and relevant recent research findings related to Tref will be highlighted. More comprehensive reviews focusing solely on Tref are available in the literature [5–9]. This review focuses on the fractionation of ethylene/α-olefin copolymers by Crystaf and Tref, because these techniques have been used more often to analyze this class of polymers. Extensions to other types of semicrystalline polymers, however, will also be discussed when required.

2 Theoretical Background

The fractionation mechanism of Crystaf and Tref relies on differences of chain crystallizabilities in dilute solution: polymer chains with high crystallizabilities will be fractionated at higher temperatures, while chains with low crystallizability are fractionated at lower temperatures. In this section, we review the basic theory of polymer crystallization in dilute solutions to explain how solvent type, polymer volume fraction, molecular weight, and comonomer content affect chain crystallizabilities and equilibrium melting temperatures. The theory describing the CCD of copolymers will also be summarized.

2.1 Thermodynamic Considerations for Homopolymer Solutions

The Flory–Huggins equation for the free energy of mixing can be used to describe the thermodynamic equilibrium of a concentrated polymer solution assuming a uniform distribution of solvent and polymer segments [10, 11]. The decrease in the equilibrium melting temperature of the polymer due to the presence of solvent and the number of chain segments is given by

$$\frac{1}{T_m} - \frac{1}{T_m^0} = \left(\frac{R}{\Delta H_u}\right)\left(\frac{V_u}{V_l}\right)\left[-\frac{\ln(v_2)}{x} + \left(1 - \frac{1}{x}\right)v_1 - \chi_1 v_1^2\right], \quad (1)$$

where T_m^0 is the melting temperature of the pure polymer, T_m is the equilibrium melting temperature of the polymer in solution, ΔH_u is the heat of fusion per repeating unit, V_u and V_l are the molar volumes of the polymer repeating unit and diluent, respectively, v_1 and v_2 are the volume fractions of the diluent and polymer, respectively, x is the number of segments, and χ_1 is the Flory–Huggins thermodynamic interaction parameter.

The crystallization step in Crystaf and Tref, however, occurs in dilute solution. Theoretically, this situation is more complicated because polymer segments are nonuniformly distributed through the solution. Strictly speaking, for dilute solutions the Flory–Huggins free-energy function shown in

Eq. 1 is no longer valid. To account for the nonuniform segment distribution, the general theory for dilute solutions, where the chemical potential of the solvent is expressed in virial form, has to be considered. Fortunately, it has been found that the change in chemical potential of the polymer with increasing dilution is so small that it does not have any appreciable effect on its equilibrium melting temperature [12]. For practical purposes, Eq. 1 is obeyed over the complete concentration range of dilutions.

To examine the effect of chain length on the melting temperature of a polymer in a dilute solution, it is appropriate to rearrange Eq. 1 as follows:

$$\frac{1}{T_m} - \frac{1}{T_m^0} = \frac{R}{\Delta H_u}\frac{V_u}{V_1}\left(v_1 - \chi_1 v_1^2\right) - \frac{R}{\Delta H_u}\left[\frac{\ln\left(v_2\right)}{r} + \frac{v_1}{r}\right]. \tag{2}$$

Here, the number of repeating units per polymer chain (r) is used instead of the number of segments (x). The second term on the right-hand side quantifies the effect of chain length, indicating that the equilibrium melting temperature decreases with a reduction in molecular weight [13]. However, this term is only important for chains with low molecular weights, as clearly

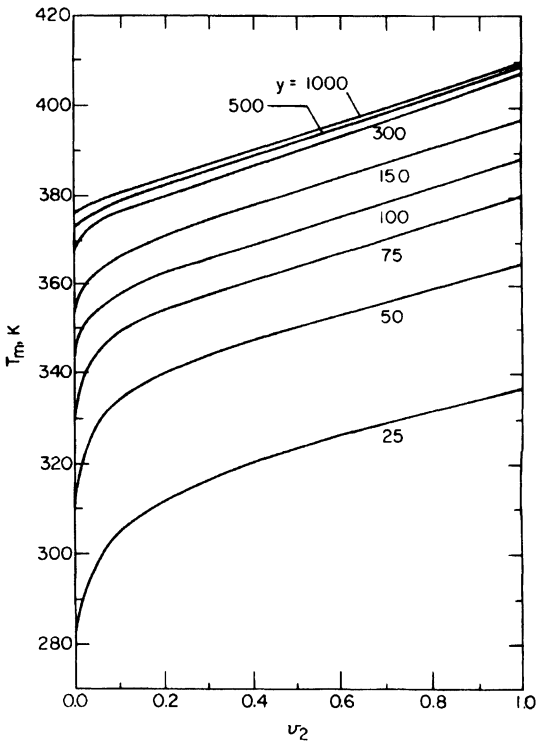

Fig. 5 Predicted melting temperatures for several chain lengths using Eq. 2 [13]

illustrated in Fig. 5. For large values of r, the case of polymers with high molecular weight, the melting temperature is relatively independent of chain length and Eq. 2 is reduced to the simpler form

$$\frac{1}{T_m} - \frac{1}{T_m^0} = \frac{R}{\Delta H_u}\frac{V_u}{V_l}\left(\nu_1 - \chi_1 \nu_1^2\right) . \tag{3}$$

Equation 3 implies that all polymer chains having reasonably large molecular weights will crystallize at the same temperature, all other factor being the same. In other words, the effect of molecular weight on Crystaf or Tref profiles of high molecular weight polymers should be negligible. This is in good agreement with experimental observations for both Crystaf and Tref [14, 24].

2.2 Thermodynamic Considerations for Copolymer Solutions

In the case of copolymer solutions, the melting temperature also depends on interactions between the different monomeric units and the solvent. Considering the case in which the crystalline phase is pure (i.e., only monomeric units of a single type crystallize and no solvent is present in the lattice), the decrease in the melting temperature can be derived in a similar manner as for the homopolymer solution case using the Flory–Huggins theory with an appropriate modification [15]. To take into account the interactions between both comonomers and solvent, the net interaction parameter for binary copolymers should be calculated as follows:

$$\chi_1 = \nu_A \chi_{1A} + \nu_B \chi_{1B} - \nu_A \nu_B \chi_{AB} , \tag{4}$$

where χ_1 is the interaction parameter of a binary copolymer with pure solvent, χ_{1A} and χ_{1B} are the interaction parameters of the corresponding homopolymers with the solvent, χ_{AB} is the interaction parameter between comonomers A and B in the copolymer chain, and ν_A and ν_B are the volume fractions of comonomers A and B in the copolymer molecules, respectively.

If the steric structures of both comonomer units in random copolymers are similar, the melting temperature depression equation will be the same as Eq. 1, with the interaction parameter calculated with Eq. 4. For a given copolymer, the crystallizabilities of copolymer chains in dilute solution strongly depend on the chain composition. From thermodynamic considerations, this can be explained from the fact that changes in copolymer composition alter the value of the interaction parameter defined by Eq. 4. For copolymers with two chemically similar comonomers, χ_{1A} will be very close to χ_{1B}, and χ_{AB} will approach zero. In this system, one can simply use Eq. 1 with $\chi_1 = \chi_{1A} \approx \chi_{1B}$.

2.3 Stockmayer's Bivariate Distribution

Stockmayer's bivariate distribution is an analytical expression describing the weight distribution of the kinetic chain length and the chemical composition for linear binary copolymers. This distribution quantifies the deviation from the average comonomer composition and molecular weight due to the statistical nature of copolymerization.

Stockmayer [16] derived this distribution with the aid of some approximations from a general theory of chain copolymerization described earlier by Simha and Branson [17]. Stockmayer's distribution has been found to be a useful tool for understanding chain microstructures of several copolymers [18–22].

Stockmayer's bivariate distribution for linear binary copolymers can be expressed by the simple equations,

$$w(r,y) = r\tau^2 \exp(-r\tau)\frac{1}{\sqrt{2\pi\beta/r}} \exp\left(\frac{-y^2}{2\beta/r}\right), \tag{5}$$

$$\beta = \overline{F}_1\left(1-\overline{F}_1\right)\sqrt{1+4\overline{F}_1\left(1-\overline{F}_1\right)\left(r_1r_2-1\right)}, \tag{6}$$

where $\overline{F}_1$ is the average mole fraction of monomer type 1 in the copolymer, y is the chemical composition deviation from $\overline{F}_1$, r is the kinetic chain length, r_1 and r_2 are the reactivity ratios for copolymerization, and τ is the ratio of the transfer rate to the propagation rate. Stockmayer's distribution was first developed from a polymerization kinetics viewpoint but a similar distribution function can also be obtained using a statistical approach [23].

This distribution function provides important insights on the detailed composition distribution of linear binary copolymers. We will use it frequently to interpret Crystaf and Tref fractionation results in the next sections of this review. Therefore, it is useful to discuss some of its main characteristics in this section.

Figure 6 shows that copolymers with a tendency to form comonomer blocks ($r_1r_2 > 1$) will have a broader CCD than copolymers having a tendency toward alternating comonomers ($r_1r_2 < 1$). Note that $r_1r_2 = 1$ is the condition of ideal copolymerization, which generates random copolymers. Considering copolymer chains with the same r_1r_2 but different chain lengths, Stockmayer's distribution shows that short copolymer chains will have a broader composition distribution than long copolymer chains (Fig. 7). These simulation results are in fact intuitive: as the chain length of a copolymer approaches infinity, its composition should approach the average copolymer composition; similarly, a tendency to form alternating comonomer units ($r_1r_2 < 1$) will forcibly result in copolymers with a 50/50 mol% comonomer composition and a very narrow CCD.

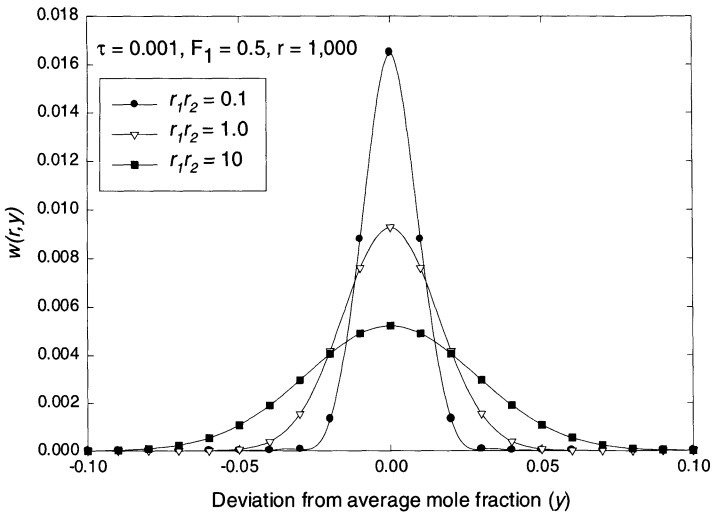

Fig. 6 Chemical composition distribution as a function of reactivity ratio product

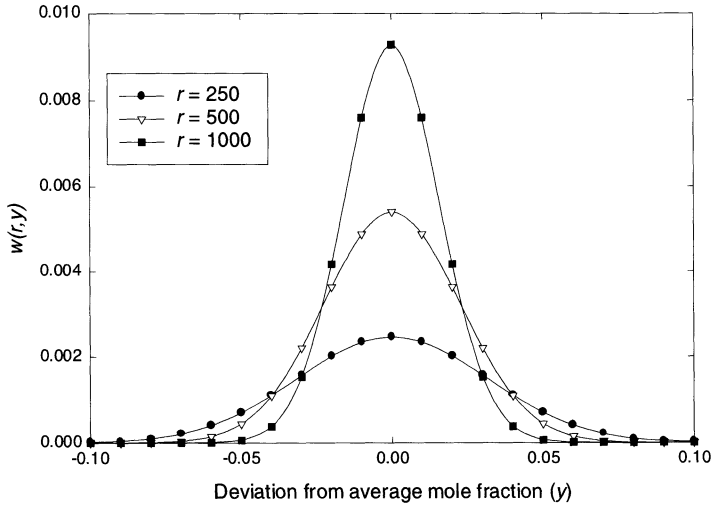

Fig. 7 Chemical composition distribution of copolymer chains with different chain lengths

Integrating Eq. 5 over all chain lengths, one obtains the equation describing the CCD component of Stockmayer's distribution, independently of chain length:

$$w(y) = \int_{r=0}^{\infty} w(r,y)\,\mathrm{d}r = \frac{3}{4\sqrt{2\beta\tau}\left(1+\frac{y^2}{2\beta\tau}\right)^{5/2}}. \tag{7}$$

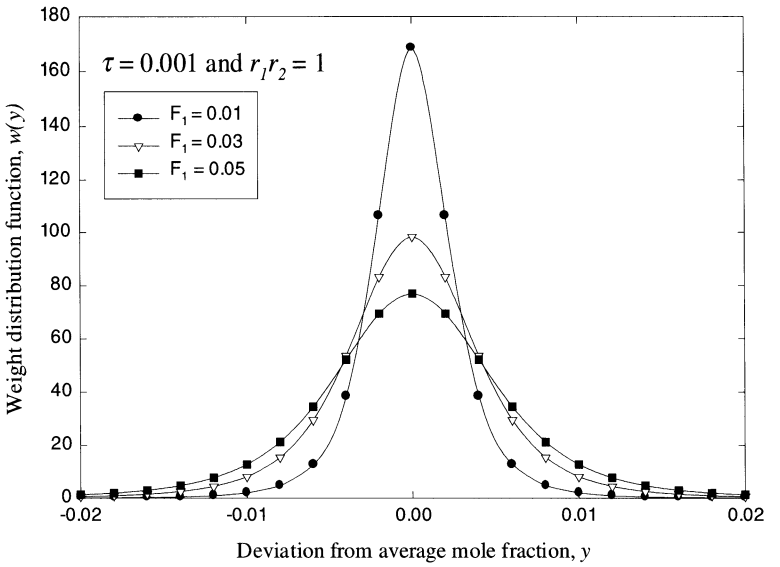

Fig. 8 Broadening of the chemical composition distribution due to increasing average comonomer content as predicted by Stockmayer's distribution, Eq. 7

Figure 8 illustrates how the CCD, predicted with Eq. 7, varies as a function of average mole fraction of monomer type 1. Notice that the CCD broadens with increasing average mole fraction of monomer type 1. This phenomenon will also be demonstrated experimentally later in this review.

3 Temperature Rising Elution Fractionation

Similarly to Crystaf, Tref is an analytical technique that fractionates semicrystalline polymers on the basis of chain crystallizabilities. However, Tref involves two consecutive steps, crystallization and elution, while Crystaf can perform a similar analysis in a single crystallization step.

Tref can be operated in analytical or preparative modes (A-Tref and P-Tref, respectively). Figures 9 and 10 show diagrams of experimental set-ups for both modes of operation [24, 25]. These two operation modes differ mainly in the elution step and sample size, which will be discussed later in more detail.

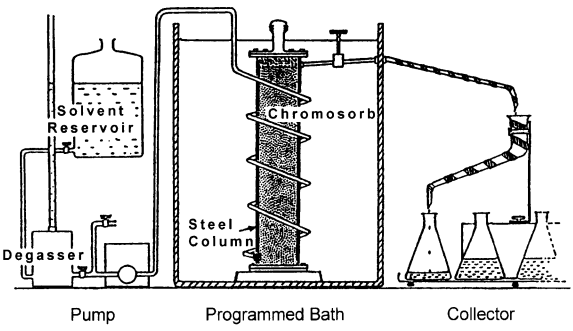

Fig. 9 Schematic diagram of preparative Tref (*P-Tref*) [25]

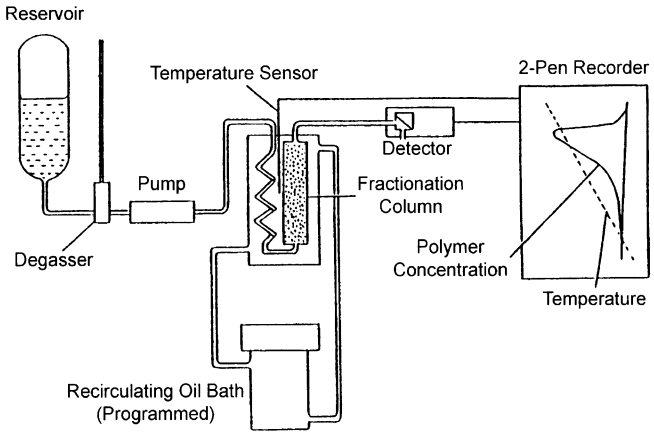

Fig. 10 Schematic diagram of analytical Tref (*A-Tref*) [24]

3.1
Basic Experimental Apparatus and Procedures

Tref operation can be briefly described as follows. First, the polymer sample is dissolved in a good solvent at high temperature and then introduced into a column containing an inert substrate, such as glass beads or steel shot. The temperature in the column is then decreased at a slow, constant cooling rate (CR). This step allows polymer chains to crystallize in an "orderly" fashion, from higher to lower crystallizabilities, i.e., from lower to higher comonomer contents. Alternatively, the crystallization step can be carried out in a temperature-programmable stirred vessel containing the inert substrate (Fig. 11) [8] and after precipitation is complete, the polymer-coated support is introduced into the Tref column. (The onion skin schematic depicted in Fig. 11 for the polymer precipitated onto the support is for illustrative purposes only; it most certainly does not correspond to the polymer phase distribution on the actual support.) For both A-Tref and P-Tref, the CR has to

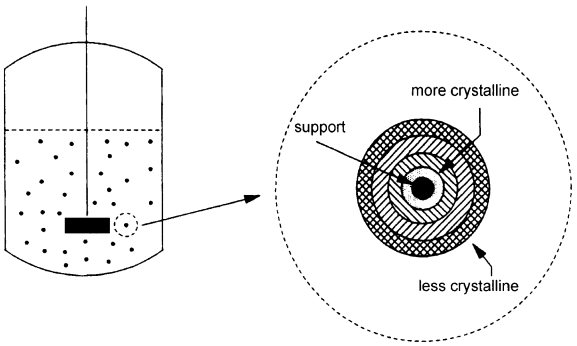

Fig. 11 Illustration of polymer layers on the support after the crystallization step in Tref. Layer dimensions are greatly exaggerated for illustration purposes [8]

be slow enough to ensure efficient polymer fractionation. The crystallization step is the most important one in Tref, as most of the polymer fractionation occurs during this period.

In the elution step, pure solvent is flowed through the column as the temperature is increased. As the dissolution temperature of the polymer is reached, the polymer outer layers dissolve back into the solvent in the reverse order they were precipitated. The elution step is carried out in different ways for A-Tref and P-Tref. Table 1 summarizes the most relevant characteristic of both methods [5].

In A-Tref, the column temperature in the elution step is increased at a slow, constant rate, while the polymer concentration in the eluent is monitored with an on-line mass-sensitive detector to obtain the Tref profile (the distri-

Table 1 Comparisons between analytical and preparative temperature rising elution fractionation (*A-Tref* and *P-Tref*) [5]

A-Tref	P-Tref
1. Fractions are collected continuously by gradually increasing the elution temperature.	1. Fractions are collected at predetermined temperature intervals. Continuous operation is less commonly used.
2. Information on macromolecular structure is obtained on-line by means of a calibration curve.	2. Information on macromolecular structure is obtained off-line by additional analytical techniques.
3. Requires smaller columns and smaller sample sizes.	3. Requires larger columns and larger polymer sample sizes.
4. Faster than P-Tref but generates less information about polymer microstructure.	4. Time-consuming but can generate detailed information about polymer microstructure.

bution of chain crystallizabilities in terms of the weight fraction of polymer eluted at each temperature). The CCD and the tacticity can be obtained from the Tref profile using a calibration curve.

P-Tref generally uses larger columns and samples sizes. In this case, the temperature is increased as a step function and all polymer eluting in a given temperature interval is recovered for further analysis by other techniques. P-Tref is more commonly used to prepare a series of fractions, each having narrower CCDs than the parent sample.

Tref can also be combined with other fractionation techniques, such as size-exclusion chromatography (SEC) or successive solution fractionation (SSF). These cross-fractionation techniques can provide a great wealth of information on chain microstructure. The applications of cross-fractionation techniques using Tref will be summarized later in this review.

3.2
Effect of Chain Microstructures and Operation Conditions

It is important to have a clear understanding on how chain microstructural characteristics and operation conditions influence Tref results in order to avoid data misinterpretation. Wild et al. [24] studied the effect of molecular weight on the fractionation process in Tref using linear polyethylene fractions with narrow molecular weight distributions (MWDs). They reported that molecular weight effects could be observed when polymers with low molecular weights (less than 10 000) were considered. Tref results become independent of chain length, however, for polyethylene samples with higher molecular weights. These experimental results are in agreement with the theory of crystallization from dilute solution discussed earlier.

Comonomer content significantly affects Tref profiles. This is to be expected, as the comonomer units are known to reduce chain regularity, thus lowering chain crystallizability [26, 27]. Linear relationships between average comonomer contents (CC) and elution peak temperatures are generally observed for ethylene/1-olefin copolymers [5, 6]. It is important that these relationships reflect only the influence of comonomer content because they are used as calibration curves to convert Tref profiles into CCDs.

Recently, Savitski et al. [28] investigated the effect of short-chain branch length on Tref using sets of ethylene/1-olefin copolymers. They reported that comonomer type could noticeably affect Tref profiles and change the slope of Tref calibration curves (Fig. 12). At the same comonomer content, the calibration curves are shifted to lower elution temperatures as the length of the short-chain branch increases. This can be explained from the fact that, as the length of the short branch increases, they become effective at disrupting the crystal regular packing and are more likely to be excluded from the lattice. Therefore, longer short branches more effectively decrease chain crystallizability. These results imply that, to estimate the CCD accurately, the branch

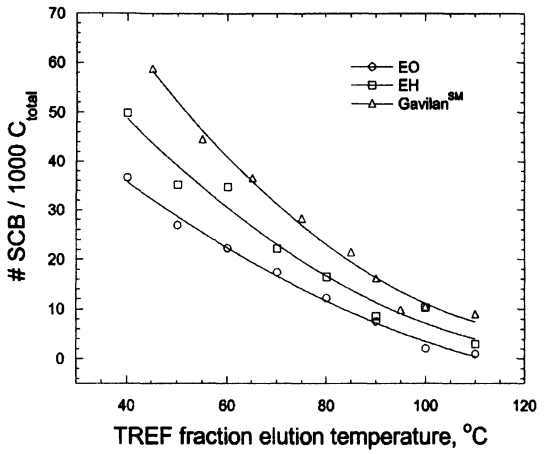

Fig. 12 Effect of comonomer type on Tref calibration curves [28]

type must be known a priori in order to choose an appropriate calibration curve.

Operation conditions also influence Tref results. Our recent work [29] showed that crystallization kinetics plays an important role in the fractionation process. The CR, the heating rate, and the solvent flow rate can affect Tref profiles to a large extent. We demonstrated that there is a general relationship between Tref profiles and the relative ratio among the CR, the heating rate, and the solvent flow rate:

1. A too fast CR can significantly reduce the fractionation efficiency, as polymer chains will not have sufficient time to separate according to their microstructures.
2. Since the solvent flow rate during the elution step determines the residence time of the polymer solution in the column, slow flow rates broaden Tref profiles and increase the Tref peak temperature, most likely due to an increase in residence time and axial dispersion in the column. Although higher solvent flow rates can help reduce axial dispersion, they also reduce the signal-to-noise ratio.
3. Fast heating rates can broaden Tref profiles, as a given volume of solvent will elute polymer over a wider range of crystallinities.

On the basis of these observations, we proposed that keeping a constant ratio of CR, heating rate, and solvent flow rate was required to cancel out the effects of the individual rates and generate very similar Tref profiles at different operation conditions. Figure 13 demonstrates that this approach is valid for the range of conditions investigated.

Cocrystallization is commonly studied by analyzing blends of two or more polymer samples. Cocrystallization is considered significant when the Tref profile for the blend cannot be superimposed onto the Tref profiles of the

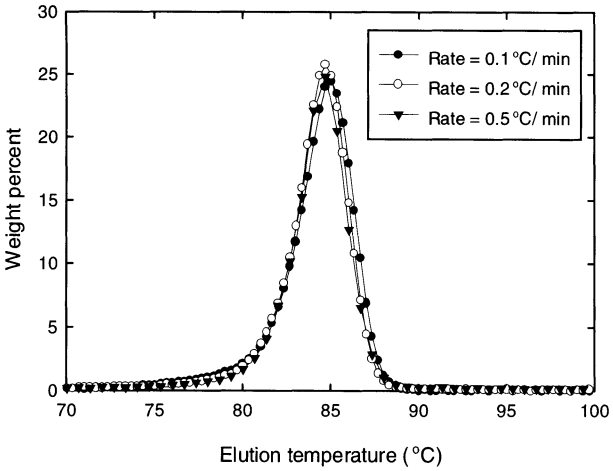

Fig. 13 Tref profiles for different operation conditions. The ratio of cooling rate : heating rate : solvent flow rate remains constant at 1 : 1 : 1 [29]

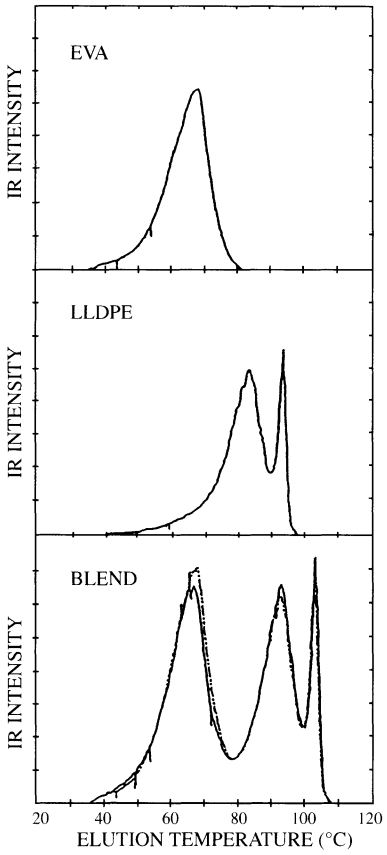

Fig. 14 Tref profiles of a polyolefin blend and its parent samples [30]

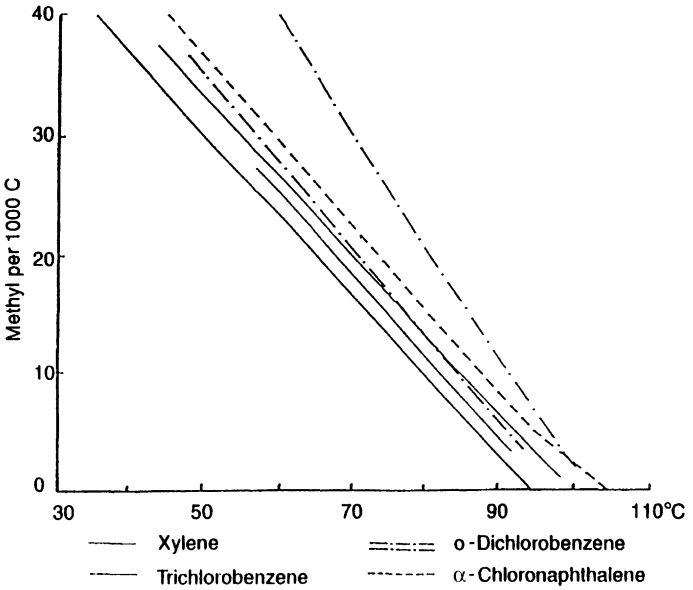

Fig. 15 Tref calibration curves for several solvent types [31]

blend components. Generally, cocrystallization during Tref analysis is reported to be very small (Fig. 14) [30]. However, our recent work [29] shows that fast CRs can promote significant cocrystallization during the analysis of ethylene/1-olefin blends, as will be discussed in more detail later in this review.

Within the range of commonly used initial polymer concentration (1–10 mg/mL), this operation parameter does not play a major role in the fractionation [29]. A high polymer concentration can help increase the signal-to-noise ratio, but too high a concentration can cause problems such as plugging of the lines, detector, and Tref column. The particular design of each Tref apparatus normally determines the range of appropriate initial concentrations.

Solvent type does not seem to affect the efficiency of the fractionation process in any significant way. Different solvent types simply shift Tref profiles to higher or lower elution temperatures depending on the interactions between polymer and solvent. Thermodynamically good solvents shift Tref profiles to lower elution temperatures, while poorer solvents do the opposite. Calibration curves prepared using different solvents were reported to be almost parallel (Fig. 15) [31], which indicates that the choice of solvent in Tref is of minor importance.

3.3
Use of Tref to Estimate the CCD of Copolymers

One of the main applications of Tref is determining the CCD of copolymers. The major difficulty of using Tref analysis to obtain quantitative CCDs is that the calibration curve depends on several operation conditions and on material type. Factors that affect Tref calibration curves are solvent type, CR, comonomer type, comonomer content, and comonomer sequence length distribution.

Comonomer type, fraction, and sequence length distribution can affect Tref calibration curves; therefore, calibration standards for samples with very broad and nonuniform CCDs, such as LLDPE made with heterogeneous Ziegler–Natta catalysts, are generally obtained by fractionating the parent resin with P-Tref. The compositions of these calibration standards have to be determined using other analytical techniques, such as ^{13}C NMR or Fourier transform IR (FTIR) spectroscopy, so that the comonomer composition versus elution temperature calibration curve can be determined for each sample type. Since this is a very time consuming method, most researchers simply opt for using calibration curves determined for similar polymers. Recently, standards made with metallocene catalysts have found wide application since they do not require fractionation by P-Tref. This approach, however, is quantitatively inaccurate when used to analyze polymers made with other cat-

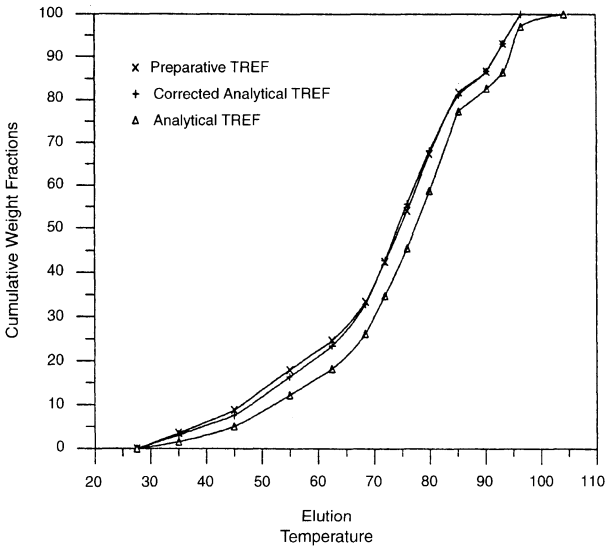

Fig. 16 Cumulative Tref profiles of A-Tref before correction, corrected A-Tref, and P-Tref [32]

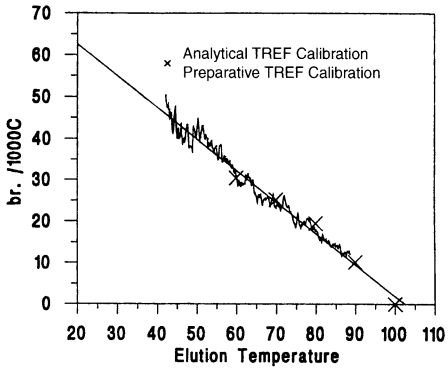

Fig. 17 Comparison between calibration curves obtained using a dual IR system in A-Tref and P-Tref [33]

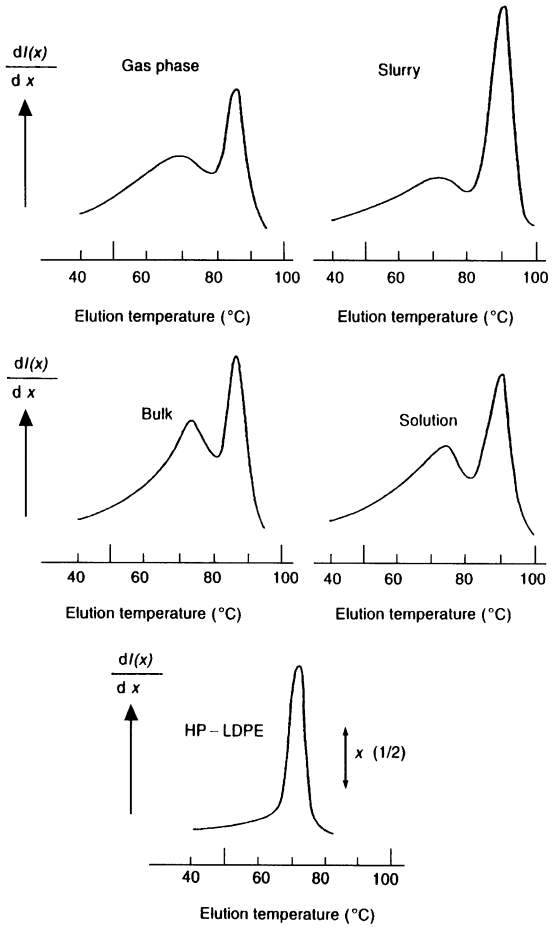

Fig. 18 Comparison of Tref profiles for LLDPE made in four different Ziegler–Natta polymerization processes and that of low-density polyethylene (*LDPE*) [34]

alysts, particularly if the "blockiness" of the sample and of the calibration standards differ considerably.

Pigeon and Rudin [32] reported the branching frequencies measured with A-Tref and P-Tref at the same elution temperature could be different (Fig. 16). Their results imply that a calibration curve produced from P-Tref cannot be used for converting raw A-Tref results to the CCD. It is necessary to correct the A-Tref results before applying the calibration curve by considering the elution time associated with the volume of the A-Tref and P-Tref columns.

To reduce the complexity of using P-Tref to obtain calibration curves, Pigeon and Rudin [33] proposed an alternative technique using A-Tref and a dual IR spectrometry detector. The dual IR system proposed allowed them to measure both concentration and branching frequency as a function of elution temperature. The calibration curve obtained by on-line dual IR spectrometry in A-Tref is identical to the one from P-Tref (Fig. 17). This eliminates the need to perform P-Tref on every sample and provides a fully quantitative Tref analysis.

Perhaps one of the greatest contributions of Tref to the understanding of olefin polymerization was the elucidation of the nature of active sites present on heterogeneous Ziegler–Natta catalysts. The systematic application of Tref to ethylene/1-olefin copolymers made with heterogeneous Ziegler–Natta catalysts in different polymerization processes has shown that all these resins have a signature bimodal Tref peak that can only be explained by the presence of two or more distinct types of active sites on the catalyst [34]. In contrast, low-density polyethylene (LDPE) made with the free-radical mechanism has a much narrower and unimodal Tref profile (Fig. 18), as expected from a free-radical polymerization mechanism.

3.4 Cross-Fractionation

Cross-fractionation is a combination of two or more fractionation techniques, each of which separates polymer chains according to a different microstructural characteristic. By combining different techniques, cross-fractionation can probe information on chain microstructure in greater detail than any single characterization technique and is an especially important tool for understanding polymers with complex chain microstructures. In this review, we considered only cross-fractionation techniques that involve chain crystallizability as one of the fractionation mechanisms. More details on a wide range of cross-fractionation techniques are available in the literature [35].

Besides being used to understand complex microstructural distributions, cross-fractionation can also be used for sample preparation. Before single-site-type catalysts were commonly available, it was extremely difficult to study the independent effect of molecular weight or comonomer composition on polyolefin properties, because polyolefins produced with Ziegler–

Natta catalysts have very broad and interdependent molecular weight and comonomer composition distributions (for these resins, the molecular weight decreases with increasing comonomer content).

SSF/solution crystallization fractionation [36] are old techniques used to prepare fractions with narrow molecular weights and comonomer composition distributions. Unfortunately, these techniques are very time consuming and generally require significant amounts of solvent. More recently, P-Tref/SEC apparatuses have been used to perform this type of cross-fractionation in a more efficient, but still rather involved, way [37–40].

In P-Tref/SEC cross-fractionation, copolymer chains are first fractionated according to comonomer composition into a series of fractions using P-Tref. Each fraction is then analyzed using SEC to obtain its MWD. P-Tref/SEC is a very powerful cross-fractionation technique because it provides information on the bivariate comonomer composition and MWD. Although the process is still time-consuming, the information obtained with P-Tref/SEC cross-fractionation provides an almost complete map of chain microstructures. This cross-fractionation technique has been used for various ethylene/1-olefin copolymers (1-butene, 1-hexene, 1-octene, and 1-pentene-4-methyl).

As is true for most complex techniques, caution should be taken when interpreting and quantifying the results from P-Tref/SEC because the fractionation mechanisms of P-Tref and SEC are not based solely on comonomer composition and molecular weight, respectively, but rather are based on chain crystallizabilities and hydrodynamic volumes.

Other common cross-fractionation techniques are SSF/A-Tref and SSF/P-Tref [41, 42]. In these techniques, polymers are first fractionated using SSF and the fractions are then further fractionated according to chain crystallizabilities using A-Tref or P-Tref. When P-Tref is used, further determination of comonomer content by ^{13}C NMR or FTIR spectroscopy is required. Figures 19 and 20 show 3D and contour plots of bivariate distributions of molecular weight and comonomer composition obtained by SSF/P-Tref cross-fractionation for an ethylene/1-pentene-4-methyl copolymer [42]. Comparing the contour plot with the equivalent contour plot of a LDPE sample (Fig. 21), one clearly notices significant differences between the bivariate distributions of these two samples.

Although the methods already mentioned can provide very detailed information on chain microstructure, they have the disadvantage of being very time consuming, which precludes their use in day-to-day analyses. Simpler approaches have been proposed by measuring one average microstructural property across the distribution of another property. For example, the average comonomer composition of polymers eluted from SEC columns can be measured as a function of molecular weight (or, more accurately, hydrodynamic volume) using on-line FTIR spectroscopy. This technique is a partial replacement for the more involved SEC/A-Tref cross-fractionation. Another possibility consists of measuring the average molecular weight of polymers

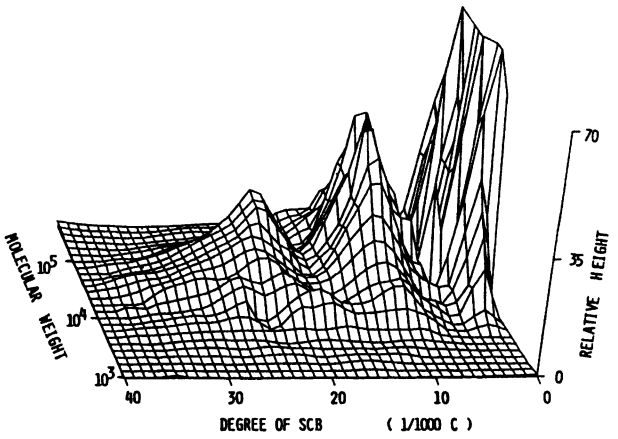

Fig. 19 Three-dimensional plot of the molecular weight distribution (*MWD*) and the CCD obtained from cross-fractionation of LLDPE [42]

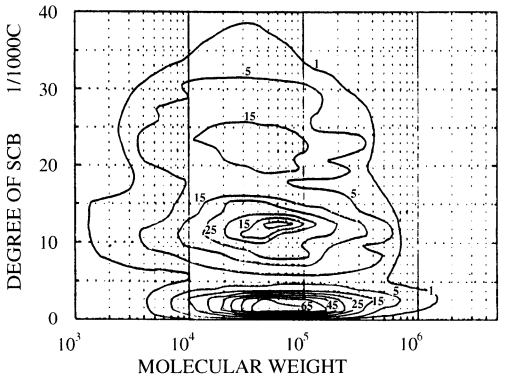

Fig. 20 Contour plot of the MWD and the CCD obtained from cross-fractionation of LLDPE [42]

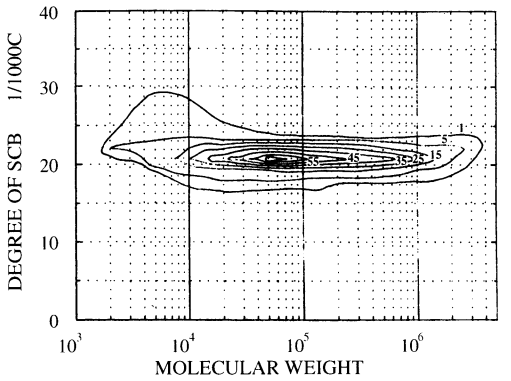

Fig. 21 Contour plot of MWD and CCD obtained from cross-fractionation of LDPE [42]

eluted from Tref columns using a light scattering detector to replace the more complex P-Tref/SEC combination. However, these two methods (SEC/FTIR and P-Tref/light scattering) are not true cross-fractionations because one of the characterization techniques merely measures average microstructural characteristics.

In the case of SEC/FTIR characterization, a method for recovering the full distribution from the average comonomer composition was proposed based on a polymerization kinetics model and the deconvolution of the MWD [43]. It was found, however, that both SEC/FTIR and P-Tref/light scattering techniques generally lose part of the information on the bivariate distribution of molecular weight and comonomer composition [44].

Besides the cross-fractionation of molecular weight and comonomer composition, another group of cross-fractionation techniques focus on the cross-fractionation of comonomer composition and chain sequence length. This group includes a combination of P-Tref and differential scanning calorimetry (DSC) with successive nucleation/annealing (SNA) [45, 46].

DSC is a widely used thermal analysis technique for studying polymer crystallization. DSC instruments contain two sample holders, each connected to their own heat source. A polymer sample is placed in one of the holders, while the other sample holder is left empty as a reference cell. By changing the temperature of both holders at a constant rate, the difference in the energy extracted from both holders to keep them at the same temperature is recorded,

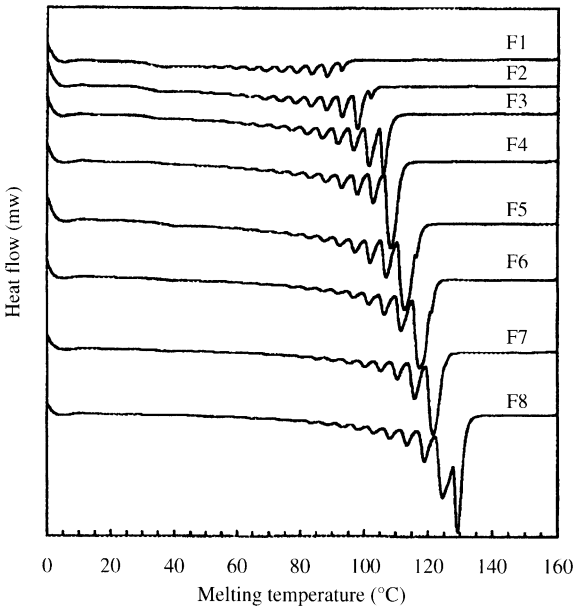

Fig. 22 P-Tref/successive nucleation/annealing cross-fractionation of Ziegler–Natta LLDPE [46]

providing the thermogram of the heat flow as a function of temperature. As the lengths of the polymer segments that can crystallize are related to the temperature, the DSC thermogram can be related to the comonomer sequence length distribution of the polymer.

When DSC is performed in SNA mode, instead of using a constant CR, the temperature program is subjected to a series of heating–annealing–cooling cycles. This process involves recrystallization and reorganization of polymer sequences and is found to be much more efficient and to offer higher resolution compared with the conventional DSC mode of operation. Therefore, P-Tref/DSC/SNA cross-fractionation is also a useful technique to understand the intermolecular and intramolecular heterogeneity of copolymers (Fig. 22).

3.5 Mathematical Modeling of Tref

Because of the complexity of the fractionation mechanism, not many mathematical models have been proposed to describe separation with Tref. Soares and Hamielec [47] used Stockmayer's distribution (Eq. 7) to simulate the CCD of linear binary copolymers synthesized with multi-site-type catalysts. Under the assumption that the fractionation process of Tref was controlled only by comonomer composition, the CCD was directly converted into the Tref profile using a calibration curve. For the case of ethylene/1-olefin copolymers made with multiple-site catalysts, the CCD of the whole polymer is described as the weighted summation of the CCDs of the copolymers produced by each active site:

$$\overline{w}(y) = \sum_{i=1}^{n} m_i w_i(y)\,, \tag{8}$$

where $\overline{w}(y)$ is the CCD for the whole polymer, m_i is the mass fraction of polymer produced on site i, $w(y)$ is the CCD for the individual site i (Eq. 7), and n is the total number of site types. Equation 8 is very useful to represent the effect of multiplicity of active sites on the CCD, but other alternative models are also possible [48]. Since Eq. 8 permits the most straightforward description for the CCD of polymers made with multiple-site catalysts, it will be the only model used in this review to illustrate Tref and Crystaf fractionation.

Figure 23 shows a simulated Tref profile for a LLDPE model sample made with a five-site-type catalyst [47]. By solving the inverse problem, this approach has been used to deconvolute experimental Tref profiles and provide information on the number of active-site types present on the catalyst (Fig. 24) [49]. This model, however, has the serious limitation of not accounting for peak broadening in Tref. Peak broadening in Tref has been reported to be significant (Fig. 25) [50].

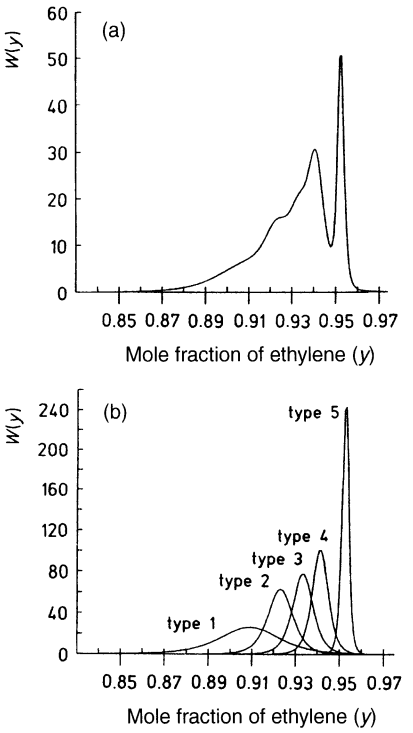

Fig. 23 (**a**) Simulated Tref profile of LDPE made by a five-site-type catalyst. (**b**) Simulated Tref profiles of LLDPE made by each catalytic-site type in a five-site-type catalyst [22]

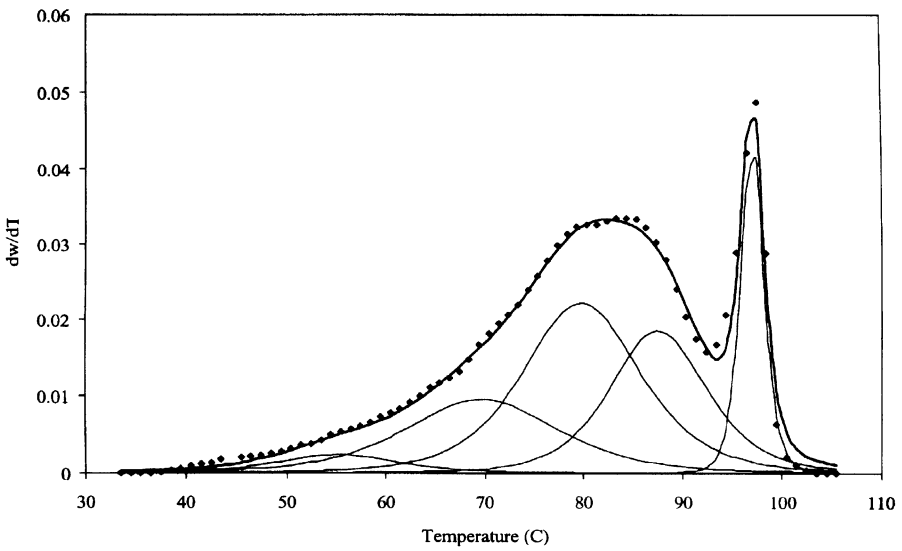

Fig. 24 Deconvolution of the CCD to determine the active-site types of a heterogeneous Ziegler–Natta catalyst [49]

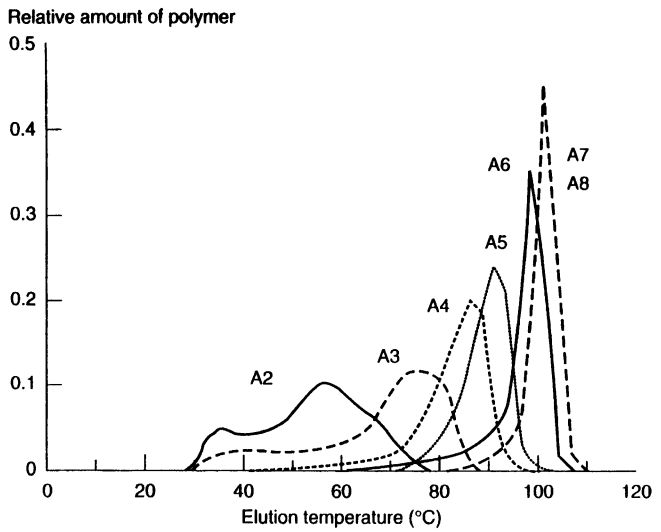

Fig. 25 A-Tref profiles of P-Tref fractions obtained at 3 °C intervals. Significant broadening can be observed [50]

Borrajo et al. [51] and Eliçabe et al. [52, 53] proposed a thermodynamic model for Tref based on the Flory–Huggins theory. They attempted to relate the distribution of crystallizable chain lengths with the elution temperature profile. Their model was validated only for the limiting case of low molecular weight high-density polyethylene (HDPE) with a narrow MWD. Since the model assumes extended-chain crystallization, it cannot adequately explain the results when long polymer chains are considered, as chain-folding effects during crystallization are found to play an important role in this case.

4
Crystallization Analysis Fractionation

4.1
Basic Experimental Apparatus and Procedures

Figure 26 shows a schematic diagram of one Crystaf crystallization vessel. The commercial version of Crystaf (Polymer *Ch*ar, Spain) has five crystallization vessels that are placed inside a temperature-programmable oven. The vessels can be used in parallel to analyze up to five samples simultaneously (Fig. 27). The vessels are made of stainless steel and are provided with stirring units. The crystallization vessels are connected to a nitrogen line, a waste line, and a sampling line attached to an in-line filter. The sampling lines are connected

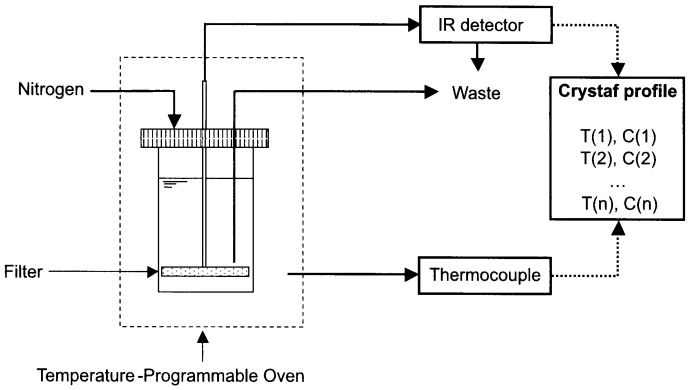

Fig. 26 Schematic diagram of a crystallization vessel in Crystaf

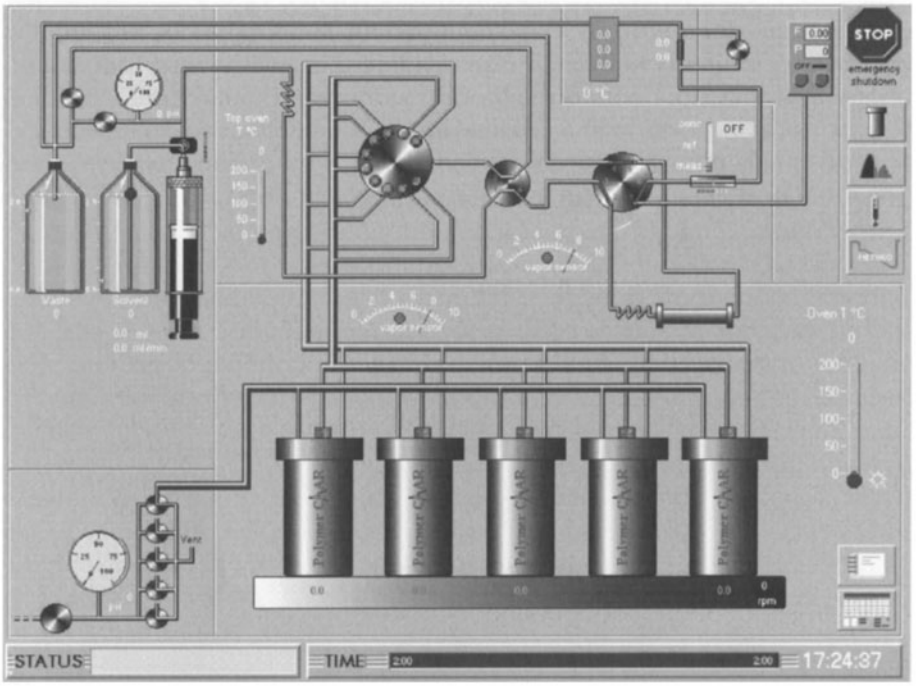

Fig. 27 Schematic diagram of a commercial Crystaf unit (Polymer *Ch*ar, Spain)

to an on-line IR detector used to measure the polymer solution concentration as a function of crystallization temperature.

Prior to the fractionation or crystallization step, the polymer sample is dissolved at high temperature in a good solvent inside a crystallization vessel to ensure complete dissolution. For analyzing polyolefins, 1,2,4-tricholobenzene is generally the solvent of choice. Dilute solutions (0.1–0.5 mg/mL) are recommended to avoid effects from chain-to-chain interactions and cocrystal-

lization, but solutions with too low initial concentrations (below 0.1 mg/mL) might lead to poor resolution owing to low signal-to-noise ratios.

The dissolution step is followed by the stabilization period, when the temperature of the polymer solution is kept a few degrees above the initial crystallization temperature. The exact value of the stabilization temperature is, of course, determined by the polymer of interest. A stirring rate of approximately 200 rpm is commonly used during both dissolution and stabilization periods; however, the stirring rate is reduced to approximately 100 rpm for the subsequent crystallization steps to minimize shear-induced chain scission. Notice, however, that a small degree of chain scission is tolerable, since Crystaf is not significantly affected by molecular weight. Stirring during the crystallization step is necessary to ensure a uniform polymer concentration distribution and avoid filter plugging.

During the crystallization step, the temperature of the solution is decreased at a slow, constant CR, typically of 0.1–0.2 °C/min. This allows the polymer chains with the highest crystallizabilities to precipitate first at high temperatures, followed by the chains with lower crystallizabilities. A slow CR is essential to minimize undesirable crystallization kinetics and cocrystallization effects. At predetermined temperature intervals during the crystallization, a small aliquot of polymer solution is removed from the crystallization

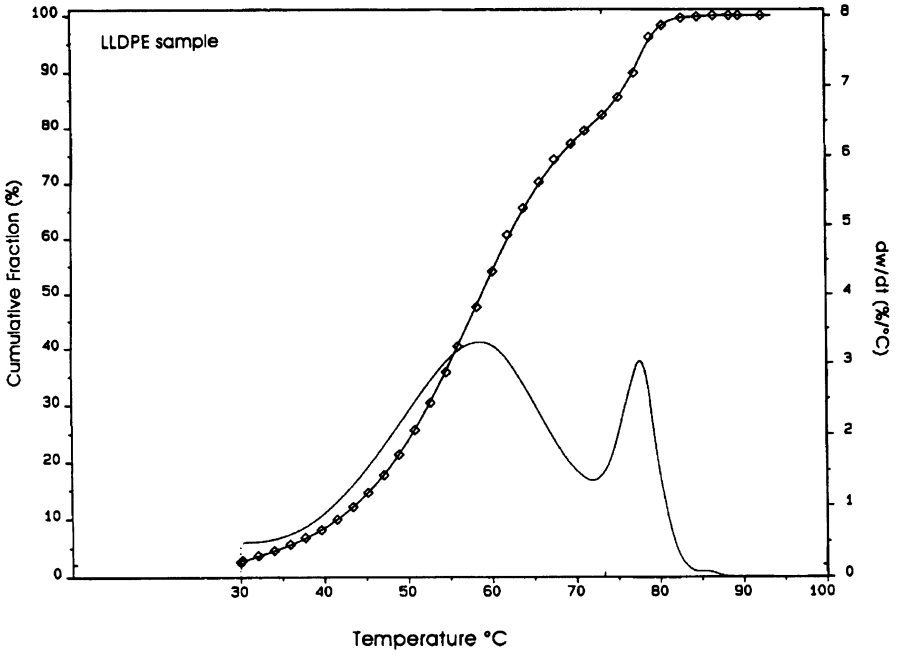

Fig. 28 Typical cumulative (or integral) and derivative Crystaf profiles of LLDPE synthesized with a Ziegler–Natta catalyst [1]

vessel by increasing the nitrogen pressure in the vessel and forcing the polymer solution through the filter. (The in-line filter in the sampling line avoids polymer crystallites from being sampled with the polymer solution.) The concentration of polymer in solution as a function of crystallization temperature is then monitored through the on-line IR detector and recorded by the data acquisition software.

The plot of solution concentration as a function of crystallization temperature is called the cumulative or integral Crystaf profile (Fig. 28) [54]. The amount of polymer crystallizing at each temperature can be determined by differentiation of the integral Crystaf profile at that temperature. The plot of the amount of polymer crystallized as a function of crystallization temperature (called the derivative Crystaf profile or simply the Crystaf profile, also shown in Fig. 28) is the most commonly reported form of Crystaf results.

4.2 Comparison Between Crystaf and Other Characterization Techniques

Crystaf has often been compared to other techniques, specifically Tref and DSC [1, 2, 54–56]. It is generally accepted that Crystaf and Tref profiles differ mainly by a temperature shift due to the supercooling effect in Crystaf, similar to what is observed between the heating and cooling cycles in DSC.

Gabriel et al. [56] compared Crystaf, Tref, and DSC profiles for LLDPE synthesized with a Ziegler–Natta catalyst (Fig. 29). Their results provide excellent validation of Crystaf analysis. Special care should be taken, however, when comparing results from different characterization techniques, because of differences in the typical operation conditions from one technique to another. The comparison with DSC is particularly difficult to make because DSC measures the heat of crystallization in the polymer melt where effects of chain

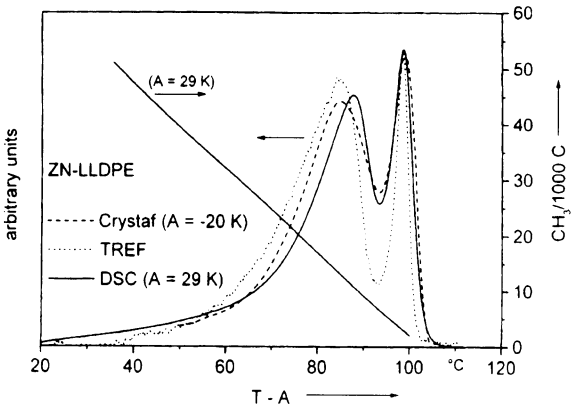

Fig. 29 Comparison of results obtained from Crystaf, Tref, and differential scanning calorimetry (*DSC*) [56]. Peaks are shifted to allow superposition

entanglement, secondary crystallization, and cocrystallization play a more important role than in Crystaf or Tref.

For some samples, the comparison between Crystaf and Tref results is not so straightforward. Britto et al. [54] compared Crystaf and Tref results for various LLDPE and HDPE samples and found that although the two techniques agreed for most samples, they could also differ for some resins at the high-crystallinity region of the profiles. Although Tref could clearly detect a high-crystallinity double peak, this peak was absent from the Crystaf profiles (Fig. 30). The appearance of this double peak may be attributed to recrystallization and also appears during DSC analyses.

To provide an unbiased comparison between Crystaf and Tref, we used these two techniques at the same CR to analyze polyolefin blends with known

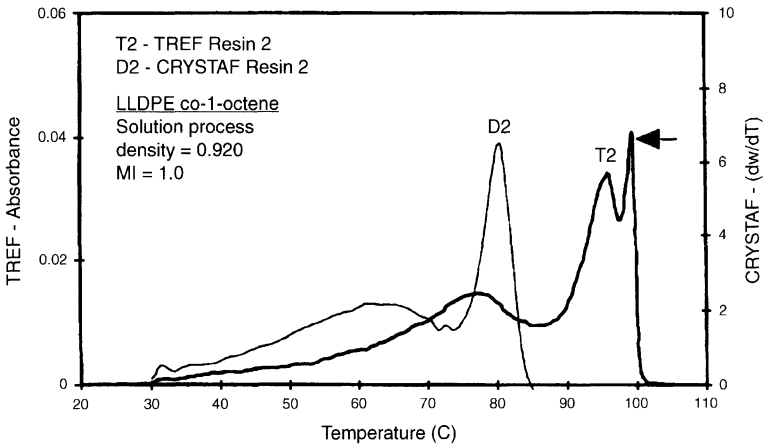

Fig. 30 Comparison between Crystaf and Tref profiles of LLDPE [54]

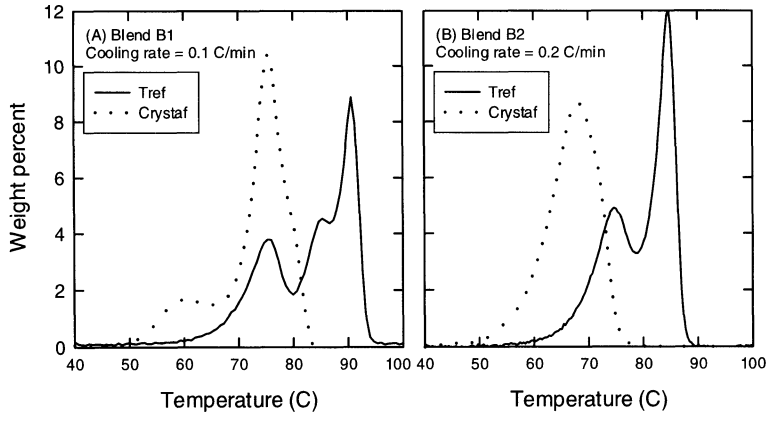

Fig. 31 Comparison between Crystaf and Tref profiles of blends of ethylene/1-hexene copolymers with known multimodal CCD measured at the same cooling rate [29]

multimodal CCDs in our recent study (Fig. 31) [29]. We found that, for the same CR, Tref can better resolve the peaks of multimodal polyolefin blends than Crystaf. It should be kept in mind, however, that the peak resolution of Crystaf can be significantly improved by using a slower CR, while still retaining the advantage of a shorter analysis time. This phenomenon will be discussed in more detail in Sect. 4.5.

Crystaf relies on the fitting (generally using splines) of 40–50 experimental points acquired for the cumulative curve. The fitted data are then used to calculate the differential Crystaf curve, as discussed before. To avoid the appearance of "false" peaks during the differentiation, curve-smoothing is sometimes required. Unfortunately, this procedure may also lead to some loss of resolution during Crystaf analysis, especially for samples containing sharp peaks. Tref is not subject to this limitation, since it directly measures the differential profile during the polymer elution step.

4.3 Effect of Chain Microstructure

All microstructural features impacting chain crystallizability can potentially influence the Crystaf fractionation process. The main microstructural properties of interest are: (1) number average molecular weight, (2) CC, and (3) comonomer type. Each of these factors will be discussed below.

4.3.1 Effect of Molecular Weight

Nieto et al. [14] investigated the effect of chain length on Crystaf profiles using a series of ethylene homopolymers with different molecular weights. A plot of Crystaf peak temperatures versus number-average molecular weights indicates that the crystallization temperature decreases with molecular weight below a certain chain length threshold (Fig. 32) [14]. However, at a reasonably high molecular weight, the crystallization temperature is independent of molecular weight. These findings are supported by the theoretical model discussed earlier for polymer solutions, as described by Eq. 2.

In addition, Crystaf profiles of polyethylene resins were reported to broaden with decreasing molecular weight averages (Fig. 33) [57], which is also in agreement with Eq. 2. As the crystallization temperature becomes independent of chain length for the samples with higher molecular weight averages, the Crystaf profiles become narrower as all chains crystallize at approximately the same temperature. On the other hand, for the samples with lower molecular weight averages, the Crystaf profiles broaden because the crystallization temperatures of the shorter chains in the sample are affected by their length.

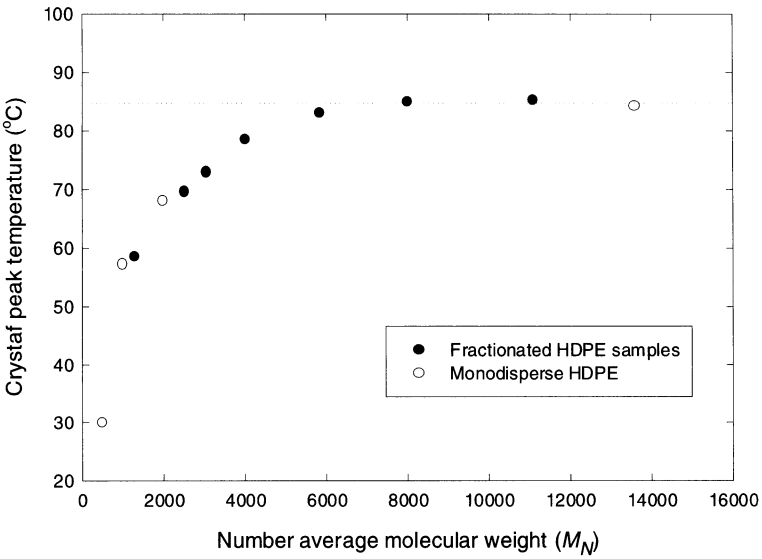

Fig. 32 Effect of chain length on the crystallization temperature of high-density polyethylene (*HDPE*) [14]

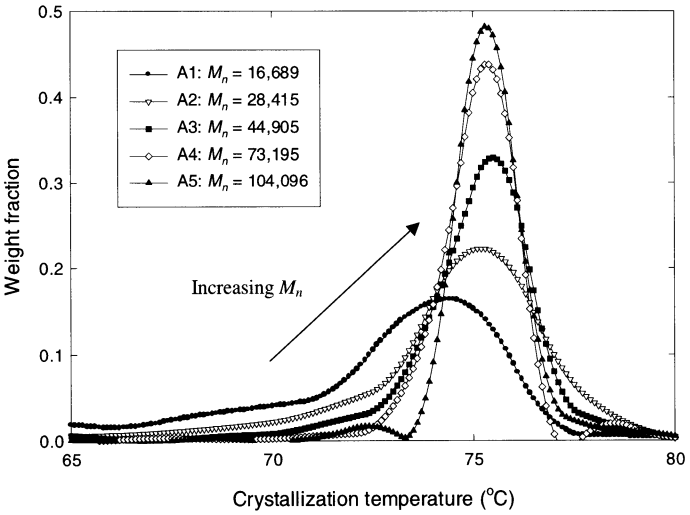

Fig. 33 Effect of number-average molecular weight on Crystaf profiles. Each sample is a fraction of ethylene/1-hexene copolymers. Fractionation was carried out using solvent/nonsolvent extraction; therefore, these samples have distinct molecular weights and contain similar amounts of 1-hexene [57]

These results have two important implications. First, Crystaf profiles will be influenced by the MWD when samples with low molecular weight averages are considered. Luckily, as shown in Fig. 33, the Crystaf peak temperature is not significantly affected unless samples with very low molecular weight aver-

ages are analyzed. This is a reassuring result, since Crystaf peak temperatures are used to create calibration curves. Second, if the sample contains chains with very low molecular weights its Crystaf profile can be significantly broadened towards the low crystallinity end of the distribution. If this factor is neglected during data interpretation and attributed to a higher fraction of comonomer, the estimated CCD will be much broader than the actual CCD.

4.3.2 Effect of Comonomer Content

The fraction of comonomer units in the copolymer chains is the most important factor affecting chain crystallizability and, therefore, crystallization temperature. This is due to the fact that comonomers act as chain defects, interrupting chain regularity and greatly lowering chain crystallizability.

Sarzotti et al. [58] investigated the effect of comonomer content on Crystaf profiles using a series of ethylene/1-hexene copolymers with different comonomer contents but approximately the same molecular weight, effectively eliminating any possible misinterpretations that might arise because of molecular weight effects (Fig. 34) [58]. As expected, Crystaf peak temperatures are dramatically influenced by the CC of the copolymer chains. Moreover, the Crystaf profiles become broader with an increase in comonomer content.

The decrease in Crystaf peak temperature can be simply explained with Eq. 4, as the chain composition alters the thermodynamic interaction parameter for the copolymer, χ_1. To understand the broadening of the distribution,

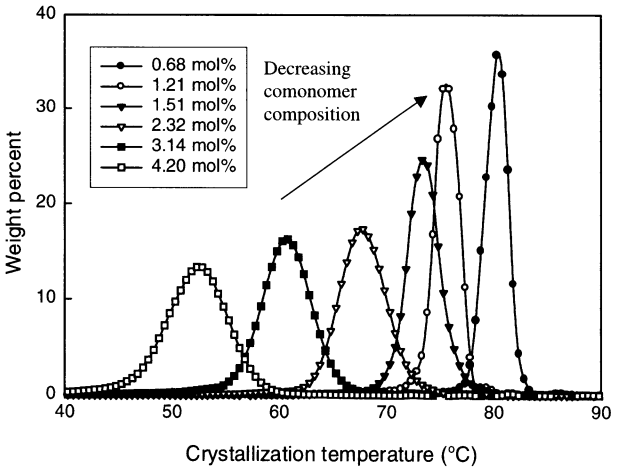

Fig. 34 Effect of comonomer content on Crystaf profiles. These samples are ethylene/1-hexene copolymers synthesized using a single-site-type catalyst. All samples have similar molecular weights [58]

however, it is more appropriate to consider Stockmayer's bivariate distribution. As previously discussed in this review, high comonomer contents will broaden the CCD of copolymers, following Stockmayer's bivariate distribution, Eq. 7. This phenomenon is elegantly illustrated in Fig. 8 from a theoretical point of view.

4.3.3 Effect of Comonomer Type

The effect of comonomer type was studied by Brull et al. [59] using propylene/1-olefin copolymers with several comonomer types (1-octene, 1-decene, 1-tetradecene, and 1-octadecene). They reported that, for their set of samples, not only Crystaf peak temperatures but also melting and crystallization temperatures measured by DSC were independent of comonomer type but depended strongly on comonomer content.

More recent work by the same research group [60] has investigated the effect of comonomer type using a series of ethylene/1-olefin copolymers (1-decene, 1-tetradecene, and 1-octadecene). Notice that ethylene instead of propylene was used in this particular study. Once more, they reported that Crystaf peak temperatures were practically independent of comonomer type (Fig. 35).

These two results are interesting because earlier work by da Silva Filho et al. [49] showed that ethylene/1-butene and ethylene/1-octene copolymers had significantly different crystallization temperatures for the same

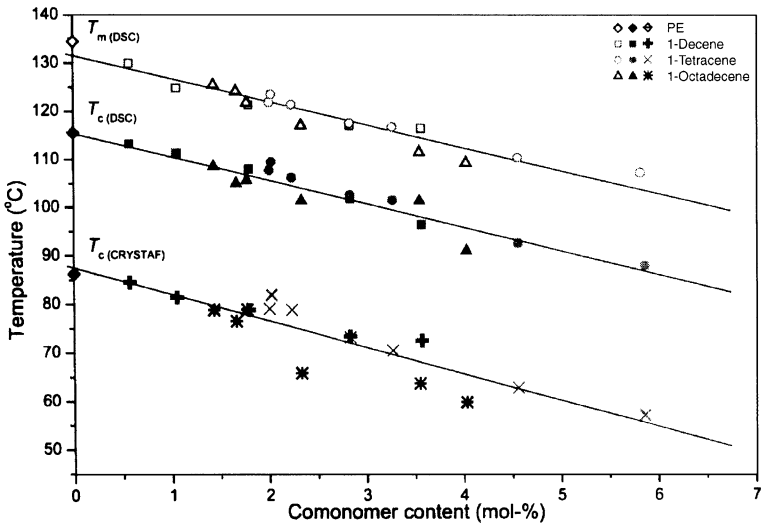

Fig. 35 Effect of comonomer type on Crystaf peak temperature and cooling and melting DSC peak temperatures [60]

comonomer content. The trend observed in their work is also in good agreement with previous investigations examining the effect of comonomer type on Tref calibration curves for ethylene/1-hexene and ethylene/1-octene copolymers (Fig. 12) [28].

Therefore, it seems that Crystaf peak temperatures are independent of comonomer type when comonomers are longer than 1-octene (1-decene, 1-tetradecene, and 1-octadecene), but depend on comonomer type for shorter comonomers (1-butene, 1-hexene, and 1-octene). We can rationalize this observation by assuming that 1-olefin comonomers longer than 1-octene are always excluded from the crystallites and therefore have the same effect on chain crystallizability. Contrarily, 1-olefin comonomers that are shorter than 1-octene can be partially incorporated into the crystallites (the shorter the comonomer, the higher the degree of crystal inclusion) and will depress the crystallization temperature to a lesser extent. This is in contrast to several experimental observations indicating that side groups larger than methyl are not significantly incorporated into the crystal structure [61–64]. It may be speculated that the comonomer effect seen in Crystaf is, therefore, related to the nonequilibrium crystallization nature of this fractionation technique.

4.4 Effect of Cooling Rate

Ideally, it would be preferable to operate Crystaf in conditions that fractionate the polymer chains according to their crystallizabilities at thermodynamic equilibrium in order to eliminate any crystallization kinetics effects. Practically, this idealized condition is untenable because very long analysis times would be required. Recent investigations [29] have shown that the fractionation process in Crystaf is, in fact, very far from thermodynamic equilibrium.

As the effect of crystallization kinetics becomes unavoidable, it is important to understand its impact on Crystaf profiles. Figure 36 shows how the Crystaf peak temperatures vary as a function of CR for three ethylene/1-hexene copolymers [29]. It is clear that the CR can have a dramatic effect on Crystaf peak temperatures even at very low CRs. The Crystaf profiles are significantly shifted to higher temperatures when slower CRs are used. Empirical linear relationships can be established between the Crystaf peak temperature of each polymer sample (T_P) and the natural logarithmic of the CR, as shown in Fig. 36.

It is important to keep in mind that the typical CR used in Crystaf analysis, 0.1 °C/min, is in fact far from thermodynamic equilibrium. This can be easily noticed as further lowering of the CR can still significantly shift the Crystaf profiles. Notice that for sample B in Fig. 36, the peak temperature is still increasing even at the prohibitively slow CR of 0.001 °C/min. Even though this should by no means be considered a limitation when comparing resins with different CCDs or measuring CCs in copolymers, it makes the development

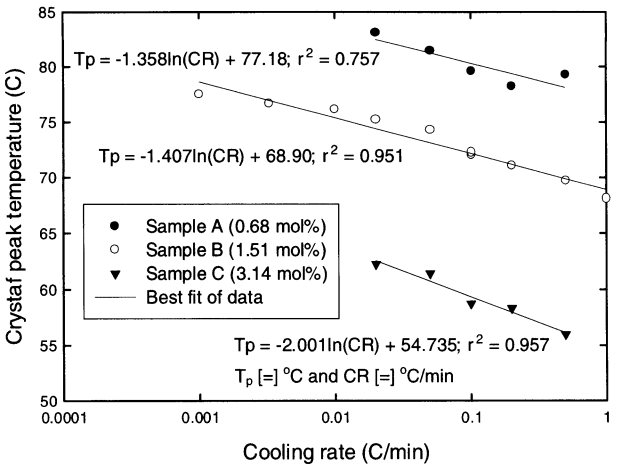

Fig. 36 Relationship between Crystaf peak temperature and cooling rate for various ethylene/1-hexene copolymers [29]

of mathematical models for Crystaf a much more challenging task since it requires that crystallization kinetics effects be taken into consideration.

4.5 Effect of Cocrystallization

Cocrystallization during Crystaf analysis can be investigated by comparing experimental Crystaf profiles of blends with their predicted Crystaf profiles, assuming the absence of cocrystallization. The Crystaf profiles of the blends in the absence of cocrystallization can be estimated as the summation of the Crystaf profiles of each parent sample, measured alone, multiplied by its weight fraction in the blend. Deviations from the predicted profile are a measure of the extent of cocrystallization taking place during the analysis.

When a blend is made of polymers with very different crystallizabilities, cocrystallization is minimal and does not have a significant effect on Crystaf profiles [1, 65, 66]. However, cocrystallization can be significant when the components of the blend have similar crystallizabilities [67]. In this case, cocrystallization can be so dramatic as to distort the shape of the measured Crystaf profile for the blend and completely mislead its interpretation.

Two factors were found to regulate cocrystallization in Crystaf: (1) CR [29] and (2) the similarity of chain crystallizabilities [67]. Figure 37 shows the effect of CR on cocrystallization of a trimodal blend of ethylene/1-hexene copolymers. Fast CRs can induce cocrystallization and distort the experimental Crystaf profile. It is important to note that this phenomenon exists even at the typically used CR of 0.1 °C.

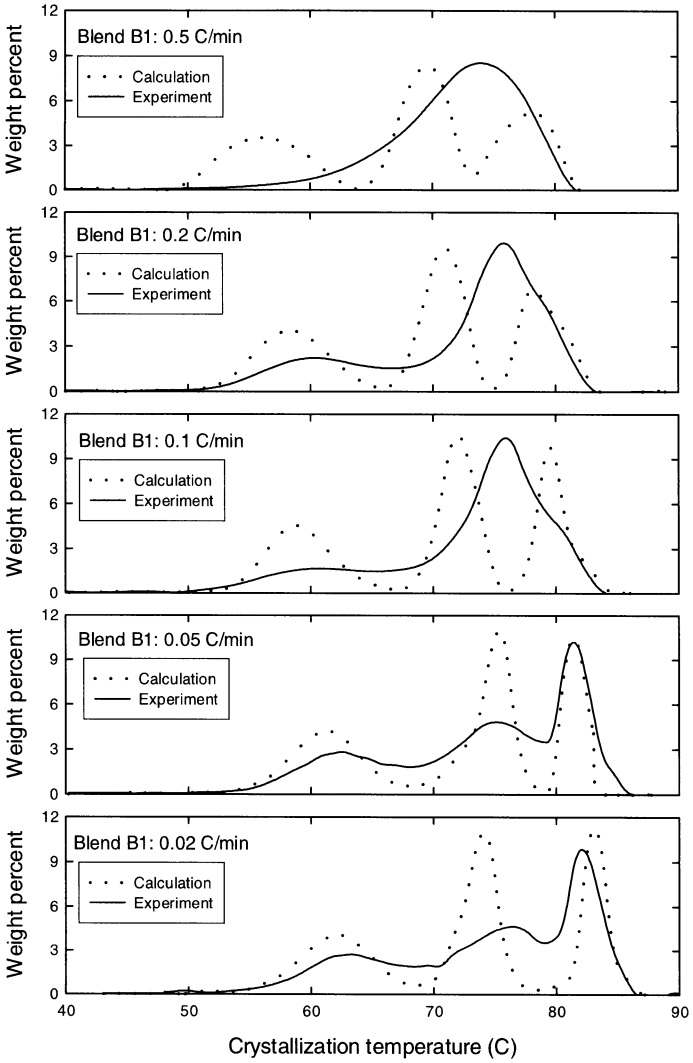

Fig. 37 Effect of cooling rate on cocrystallization during Crystaf analysis [29]

Another important factor affecting cocrystallization is the similarity of chain crystallizabilities, which can be quantified by the difference between the Crystaf peak temperatures of the parent samples, ΔT_C. By varying ΔT_C, changes in cocrystallization behavior can be easily observed (Fig. 38). Similarity of chain crystallizabilities, as indicated by a small ΔT_C, strongly induces cocrystallization during the analysis; a similar criterion could have been defined using density or crystallinity differences to access the importance of cocrystallization for these polymers.

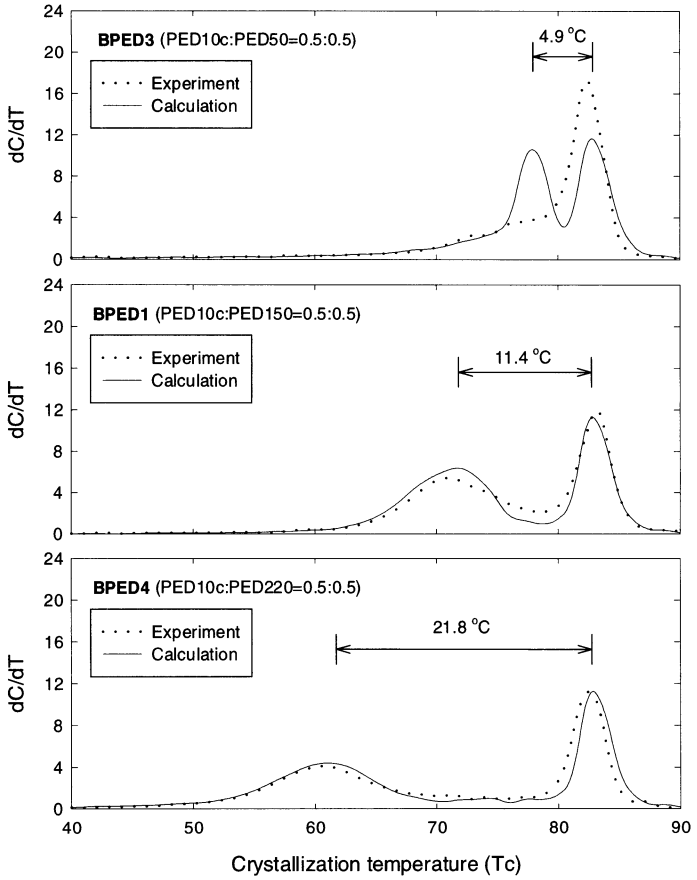

Fig. 38 Similarity of chain crystallizabilities (measured as Crystaf peak separation) induces cocrystallization in Crystaf analysis [67]

In our recent work [67], we investigated the effect of comonomer type on cocrystallization using a series of ethylene/1-olefin copolymers with four comonomer types: propylene, 1-hexene, 1-octene, and 1-dodecene. Four blends, one for each copolymer type, were prepared such that they crystallized at the same temperature range and had similar ΔT_C to eliminate the effect of similarity of chain crystallizabilities. The Crystaf results of these blends indicated that the comonomer type of the parent samples did not appreciably influence their cocrystallization behavior, as illustrated in Fig. 39.

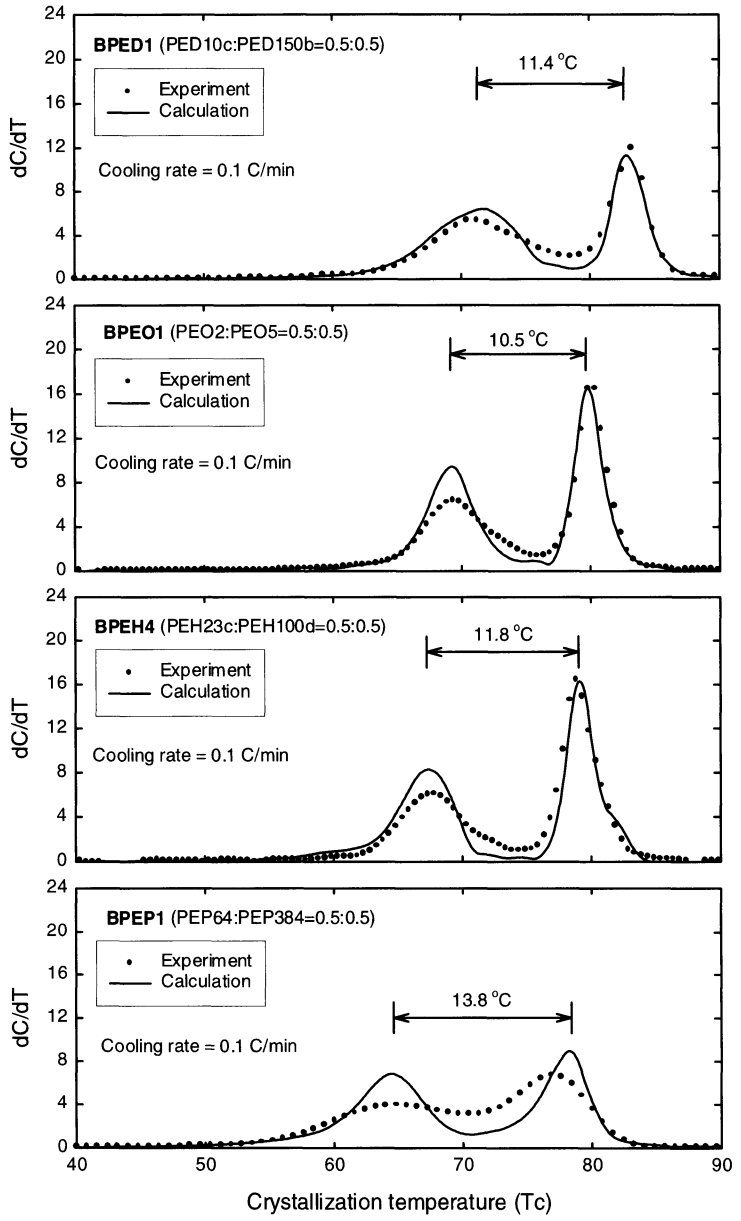

Fig. 39 Effect of comonomer type on cocrystallization at a cooling rate of 0.1 °C/min for blends with the same comonomer type. *BPED* blend of ethylene/1-dodecene copolymers, *BPEO* blend of ethylene/1-octene copolymers; *BPEH* blend of ethylene/1-hexene copolymers, *BPEP* blend of ethylene/propylene copolymers [67]

5
Crystaf Applications

5.1
Estimation of CC and CCD of Copolymers

One of the main applications of Crystaf analysis is the estimation of the CCD of semicrystalline copolymers, specifically LLDPE. The CCD of copolymers can be obtained from the Crystaf profile with the help of a calibration curve relating the CC and the crystallization temperature. For routine analysis, a calibration curve can also give a quick estimation of the CC from the Crystaf peak temperature. Evidently, because of the crystallization kinetics and cocrystallization effects described before, in general only an approximation of the actual CCD is possible with Crystaf and Tref.

Two methods for preparing the calibration curve have been reported. Both methods were done by performing Crystaf analysis in a series of narrow-CCD copolymer samples with known comonomer contents with crystallizabilities covering a broad range of crystallization temperatures. The only difference between these two methods is the type of samples used in the calibration. The first method uses a series of polymer samples synthesized with single-site-type catalysts [58, 68], while the second method uses a series of fractions from broad-CCD Ziegler–Natta copolymers obtained with P-Tref [1, 49]. After the whole series of samples has been analyzed, the relationship between Crystaf peak temperature and CC is used as the calibration curve.

A number of calibration curves have been reported for Crystaf (Table 2, Fig. 40). Unfortunately, similar to calibration curves for Tref, calibration curves for Crystaf depend on polymer type, solvent type, CR, and method of sample preparation. Published calibration curves should only be used if care is taken in trying to replicate as closely as possible the conditions under which they were obtained.

The calibration curve is significantly influenced by the CR, as should be expected from our previous discussion. We have recently proposed the following generalized calibration curve for random ethylene/1-hexene copolymers taking into account the effect of the CR [29],

$$\mathrm{CC} = 10.0 - 0.1216 \times T_\mathrm{P} - 0.1653 \times \ln(\mathrm{CR}), \tag{9}$$

where CC is in mole percent, T_P is the Crystaf peak temperature in degrees Celsius, and the CR is in degrees Celsius per minute. This empirical equation was fitted using the data from Sarzotti et al. [58] and Anantawaraskul et al. [29] and it is applicable for CR = 0.003–2 °C/min and CC = 0.68 – 4.2 mol %. The equation fits well all the experimental data with a coefficient of determination (r^2) of 0.993.

With the help of a calibration curve, Crystaf profiles can be converted to the CCD. This quantitative CCD is useful for establishing structure–property

Table 2 Summary of reported calibration equations with their applicable ranges and experimental conditions

Copolymer	Method of preparing calibration samples	Range of applicable comonomer content (mol %)	Cooling rate (°C/min)	Calibration equation	Reference (best linear fit)
PE/1-octene	Fractionation using P-Tref	0.86–4.66	0.2	$CC = -0.0968\ T_C + 8.6321$	Monrabal [1]
PE/1-octene	Synthesis using single-site-type catalysts	0.637–6.985	0.2	$CC = -0.1651\ T_C + 13.684$	Monrabal et al. [64]
PE/1-octene	Fractionation using P-Tref	0.3–6.4	0.2	$CC = -0.1248\ T_C + 10.633$	da Silva Filho et al. [48]
PE/1-hexene	Synthesis using single-site-type catalysts	0–4.234	0.1	$CC = -0.1270\ T_C + 10.86$	Sarzotti [57]
PE/1-butene	Fractionation using P-Tref	1.2–8.9	0.2	$CC = -0.1690\ T_C + 14.36$	da Silva Filho et al. [48]
PP/1-olefin	Synthesis using single-site-type catalysts	0–3.43	0.1	$CC = -0.0670\ T_C + 4.7074$	Brull et al. [58]

PE polyethylene, *PP* polypropylene

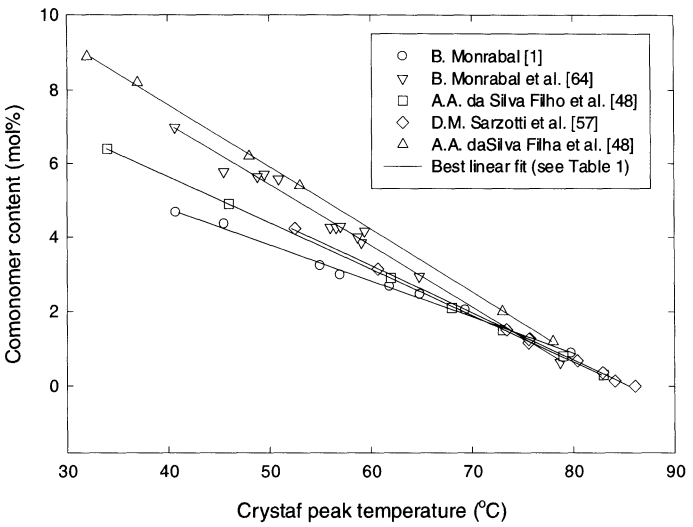

Fig. 40 Calibration curves reported for ethylene/1-olefin copolymers (see Table 2 for details of applicable range and conditions)

relationships [69, 70] and elucidating several issues in polymer reaction engineering.

5.2 Polymer Reaction Engineering

Tref has been used for many years in polymer reaction engineering investigations. For instance, Tref was one of the most important analytical techniques to determine the presence of multiple-site catalysts on heterogeneous Ziegler–Natta catalysts used for olefin polymerization, as previously illustrated in Fig. 18. Crystaf, with a much shorter analysis time than Tref, permits the routine determination of the CCD in polymer reaction engineering projects.

CCDs obtained with Crystaf have shed light on various topics in the area of polymerization and polymer degradation mechanisms. Similarly to Tref, Crystaf can be used to identify the nature of active site types in Ziegler–Natta catalysts, as proposed by da Silva Filho et al. [49].

Crystaf has been used to provide important insights on polymerization conditions affecting CCD [71–78]. For example, Fig. 41 shows how the CCD of ethylene/1-hexene copolymers made with a silica-supported binary metallocene catalyst is influenced by the relative amounts of each metallocene in the mixture [74]. This understanding leads to the ability to manipulate the CCD and allows us to tailor-make copolymers with predetermined microstructures through the combination of catalysts, cocatalysts, and/or support treatments.

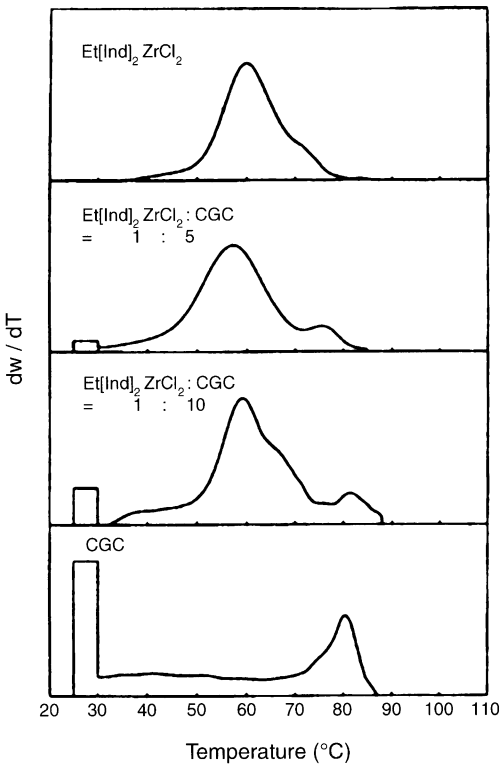

Fig. 41 Effect of catalyst type and catalyst combinations on the CCDs of ethylene/1-hexene copolymers measured by Crystaf [74]

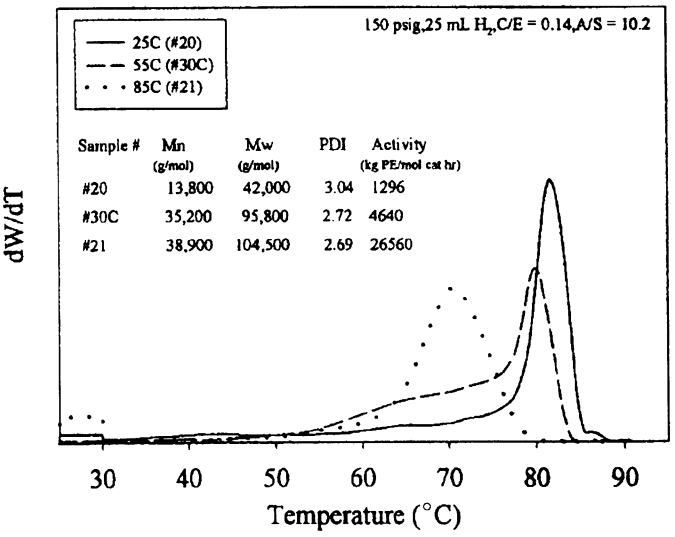

Fig. 42 Effect of polymerization temperature on the CCD of ethylene/1-hexene copolymers as measured by Crystaf [78]

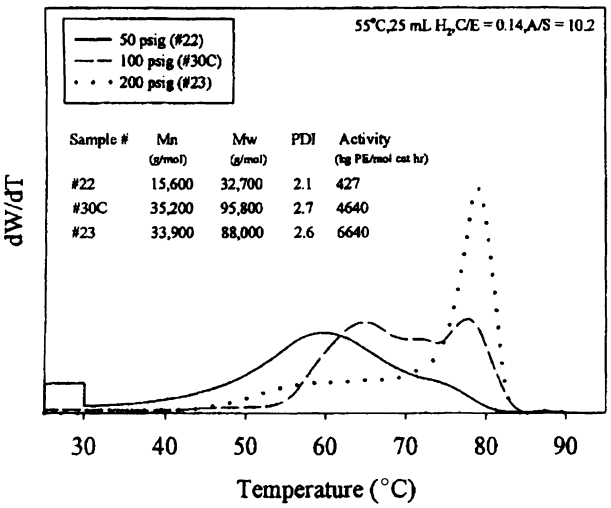

Fig. 43 Effect of polymerization pressure on the CCD of ethylene/1-hexene copolymers measured by Crystaf [78]

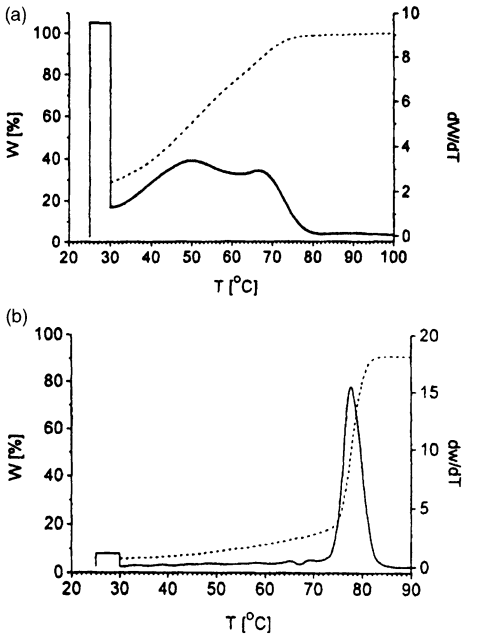

Fig. 44 Broadening of chemical heterogeneity due to thermo-oxidative degradation as revealed by Crystaf: (**a**) PP held at 110 °C for 4 days; (**b**) PP held at 130 °C for 1 day [79]

Using a careful factorial experimental design, the effect of polymerization temperature, polymerization pressure, amount of hydrogen, and the comonomer-to-monomer feed ratio on Crystaf profiles can be identified [78].

Figures 42 and 43 show the effect of polymerization temperature and pressure on the Crystaf profiles of ethylene/1-hexene copolymers produced with an in situ supported Ni diimine catalyst in the presence of chain-walking.

Recently, Crystaf has also found applications in the area of polymer degradation. de Goede et al. [79] used Crystaf to monitor the change in chemical heterogeneity during the thermo-oxidative degradation of polypropylene. Crystaf clearly reveals the broadening of chemical heterogeneity, decreasing of peak crystallization temperature, and increasing of the amount of the soluble fraction, as the degradation proceeds (Fig. 44). Crystaf analysis of the polymer taken at different distances from surface of the sample can additionally provide information about the gradient of degradation from the surface to the core of the sample, thus quantifying the spatial heterogeneity of the degradation process.

5.3 Analysis of Blend Compositions

Although several previous investigations considered the Crystaf analysis of blends, they merely intended to quantify the limitations of Crystaf due to cocrystallization [1, 2]. Only more recently has Crystaf been used to provide quantitative information on blend compositions [55, 65, 66].

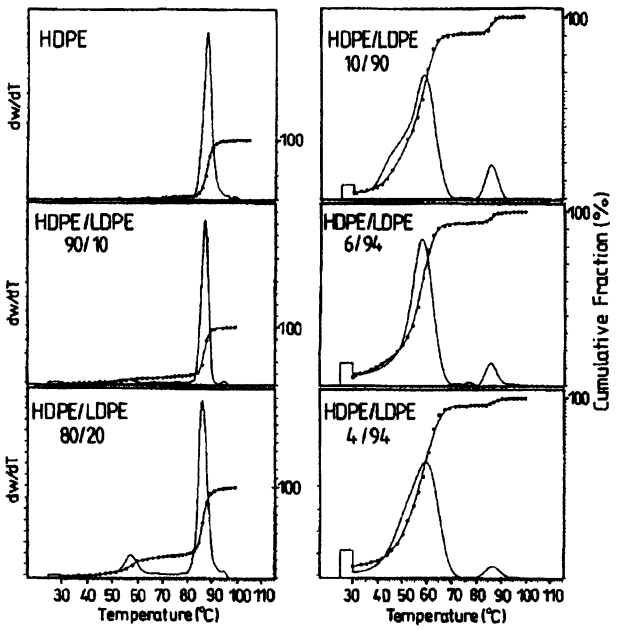

Fig. 45 Crystaf analyses of blends of commercial HDPE and LDPE [55]

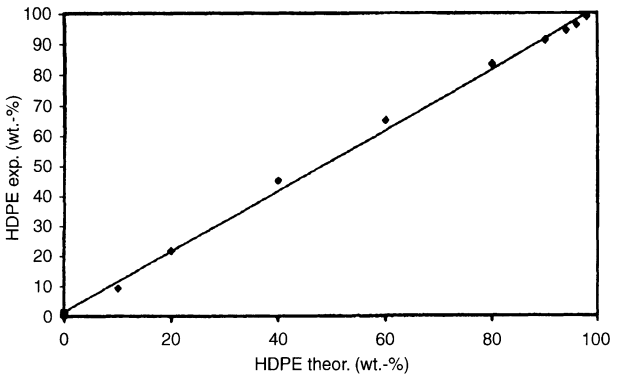

Fig. 46 Comparison between known HDPE composition in HDPE/LDPE blends and the ones measured by Crystaf [55]

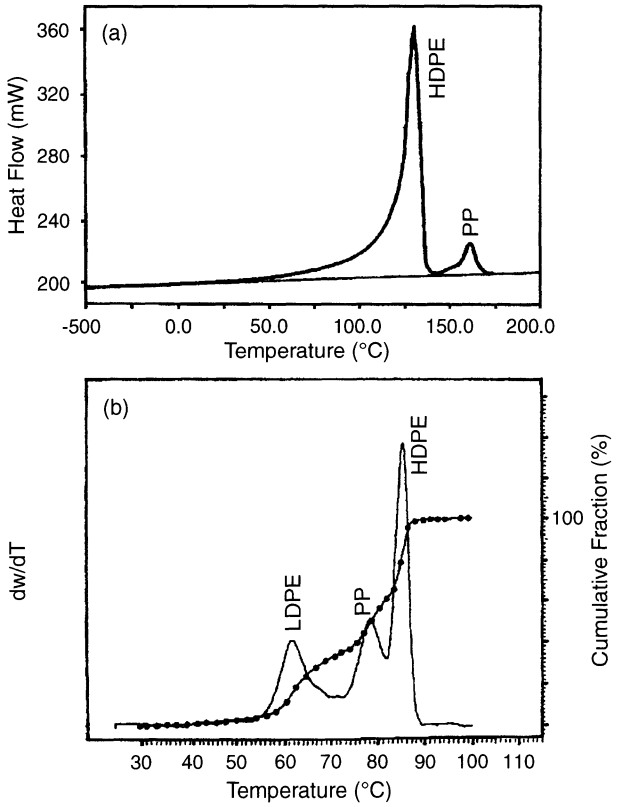

Fig. 47 DSC and Crystaf analysis of waste plastics [55]

Figure 45 shows Crystaf analyses of blends of commercial HDPE and LDPE reported by Pasch et al. [55]. By comparing the known composition of the blends with the composition measured by Crystaf (Figs. 45, 46), they

found that Crystaf was quantitatively accurate over a very wide range of compositions. For instance, Crystaf could detect blend components present in amounts as small as 5 wt %. In the analysis of waste plastic samples, Crystaf was found to be better than the conventional DSC method for providing information on blend compositions (Fig. 47).

The application of Crystaf analysis for detecting blend composition is, of course, limited by cocrystallization, particularly if accurate quantitative information is required. As previously discussed, cocrystallization is found to be significant when two chain populations crystallize at relatively close temperature ranges (small ΔT_C), even for very slow CRs. Therefore, the use of Crystaf for determining blend compositions will be more adequate when the blend components have distinctly separated Crystaf peak temperatures (large ΔT_C). Preferably, the difference between Crystaf peak temperatures should be more than 10 °C, particularly in the case where the blend components have similar molecular structures.

6
Mathematical Modeling of Crystaf

Although Crystaf has been established as a good alternative to Tref during the last decade, accurate quantitative models for describing the Crystaf fractionation process are still unavailable. Incidentally, they are equally unavailable for Tref. The main difficulty in achieving a generalized mathematical model is the complexity of the crystallization mechanism and fractionation process taking place in these two techniques, as discussed at length in this review.

Two main approaches have been proposed to model Crystaf fractionation: (1) models based on Stockmayer's bivariate distribution [58, 80], and (2) models based on the distribution of chain crystallizabilities using Monte Carlo simulation [57, 81].

6.1
Stockmayer's Bivariate Distribution Models

Sarzotti et al. [58] used Stockmayer's distribution, Eq. 7, and a calibration curve to model Crystaf profiles (Fig. 48). The two variables in Eq. 7, $\overline{F}_1$ and τ, were used as adjustable parameters to minimize the sum of the squares of the residuals between model and experimental profiles. Even though the model fitted the experimental profiles adequately, the molecular weights calculated from the model (easily obtained as $1/\tau$) were significantly lower than the ones measured by SEC, indicating that the model was not theoretically sound and only worked as a convenient empirical fit of the experimental data.

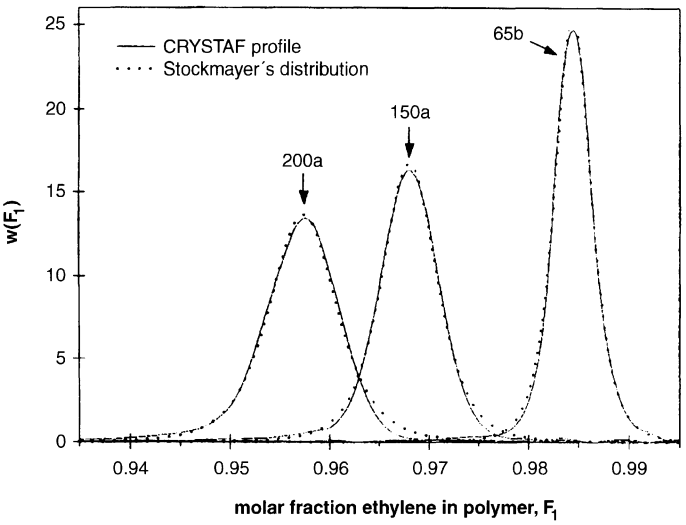

Fig. 48 Comparison between experimental Crystaf profiles and Stockmayer's bivariate distribution [58]

Soares et al. [80] proposed a model using Stockmayer's distribution with additional help from a generic instrumental spreading function to account for the instrumental peak broadening in Crystaf. Again, although the model could fit the experimental profiles well, the parameters used in the spreading function were considered purely empirical.

Although these models are not rigorously correct, the fact that they can fit well the experimental profiles is surprising, considering that using Stockmayer's distribution to model the CCD obtained from Crystaf is based on a number of rather severe simplifying assumptions. These models assume that (1) the polymer is prepared under uniform polymerization conditions (i.e., in the absence of compositional drift and other reactor nonuniformities), (2) the fractionation process in Crystaf is controlled only by the average copolymer composition per chain, (3) cocrystallization is absent during the analysis, (4) the fractionation process is independent of molecular weight even for the short chains, and (5) crystallization kinetics does not influence Crystaf profiles or, in other words, the fractionation takes place at thermodynamic equilibrium.

Unfortunately, most of these assumptions have recently been proved to be inaccurate [14, 29]. Even though modeling Crystaf profiles with Stockmayer's distribution can provide an adequate fit of the data, these models are, at best, only semiempirical. It is clear that a truly phenomenological model of the Crystaf fractionation process is essential to obtain the details of the correct distribution.

6.2 Monte Carlo Models

Monte Carlo simulation is a technique for solving stochastic problems that is widely used in the area of polymer science and engineering. Specifically for studies of polymer microstructures, it has been used to predict the CCD of copolymers and the distribution of stereoregularity [82, 83]. One of the advantages of this technique is that one can obtain detailed statistical information of chain structures simply from relatively easy to measure polymer properties such as the CC and the molecular weight.

Beigzadeh et al. [81] proposed the first Monte Carlo model for simulating Crystaf profiles. They assumed that the crystallization of a copolymer chain during Crystaf was solely governed by the length of its longest crystallizable monomer sequence. For the particular case of ethylene/1-olefin copolymers, the longest ethylene sequence per chain was assumed to govern the crystallization process in Crystaf. They proposed that Crystaf profiles could be calculated from the distribution of the longest ethylene sequence, instead of the CCD, and used Monte Carlo simulation to obtain this distribution. A modified Gibbs–Thompson equation [81] was used as the thermodynamic equilibrium relationship between the crystallization temperature and the length of the longest ethylene sequence, which was assumed to be proportional to the lamella thickness

$$T_C = \frac{T_S^\circ(LS - \alpha)}{LS} - \beta, \tag{10}$$

where T_C is the crystallization temperature measured by Crystaf, T_S° is the equilibrium melting temperature of a chain with infinite chain length, α is a constant proportional to $1/\Delta H_u$, LS is the longest ethylene sequence, and β is the supercooling temperature in Crystaf.

They obtained good agreement with the experimental Crystaf profiles for their limited sample set of ethylene/1-octene copolymers. Later, Costeux et al. [23] derived an analytical expression for this distribution of the longest monomer sequences. This analytical solution can be used to dramatically shorten the computational time required for Crystaf modeling using the method of Beigzadeh et al. [81].

The model of Beigzadeh et al. was later applied to a series of ethylene/1-hexene copolymers covering a wider range of molecular weights and comonomer contents [57]. Unfortunately, it was found that the model based on the distribution of the longest monomer sequences could not accurately describe all the resins investigated.

We proposed a modified Monte Carlo model [57] based on the distribution of average ethylene sequence lengths, which was found to better represent the Crystaf profiles for a wider range of ethylene/1-olefin copolymers. Figure 49 compares the experimental Crystaf profiles with results from the proposed

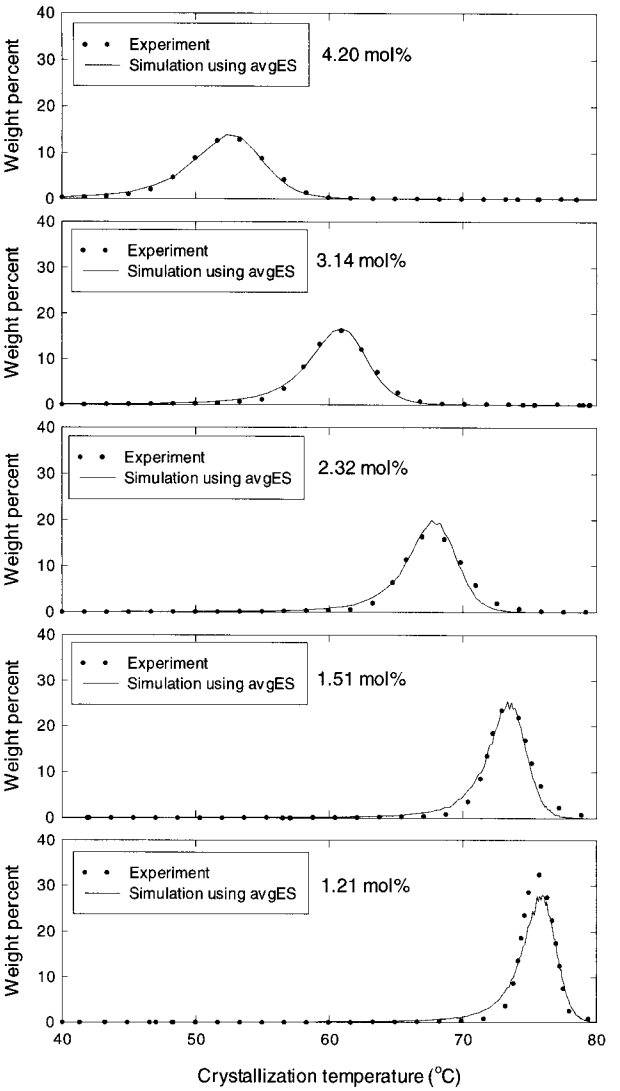

Fig. 49 Comparison between experimental and simulated Crystaf profiles of ethylene/1-hexene copolymers with different comonomer contents [57]

model. It was speculated that the distribution of average ethylene sequence lengths might provide a better representation of Crystaf profiles owing to the fact that Crystaf fractionation takes place far from thermodynamic equilibrium. In this way, using the average ethylene sequence lengths instead of the longest ethylene sequence lengths would be an indirect (and clearly empirical) way of accounting for the complex phenomena taking place during crystallization in Crystaf.

Although these Monte Carlo models can explain qualitatively the effects of molecular weight and comonomer content on Crystaf profiles, they are unable to take into account crystallization kinetics and cocrystallization effects that have recently been reported as significant factors affecting Crystaf profiles [29, 67]. More work is required to quantify these important effects. Such a model, if developed, would be invaluable to obtain a universal calibration curve for Crystaf and Tref.

7 Conclusion and Future Trends

After only approximately a decade since it was developed, Crystaf has become one of the most important analytical techniques in polyolefin characterization laboratories. It can provide fast and crucial information required for the proper understanding of polymerization mechanisms and structure–property relationships. In industry, it has been established as an indispensable tool, together with Tref, for product development and product quality monitoring.

Nonetheless, compared with its older cousin Tref, Crystaf is still in its early stage of development. Improvements not only in terms of a better theoretical understanding, but also from the viewpoint of instrumentation, might lead to a more efficient fractionation process. For example, the recent development of a triple detector (IR/light scattering/viscometer) for Crystaf, the so-called Crystaf 3D, can provide a wealth of information on polymer microstructure at each crystallization temperature.

So far, Crystaf has been mostly limited to the analysis of LLDPE and some polypropylene resins. Certainly, there are many other semicrystalline copolymers that could greatly benefit from the information on CCD provided by Crystaf. In fact, the direct extension of Crystaf analysis for these polymers might be expected in a short time, considering the easy and fully automated use of Crystaf.

Crystaf has also started to gain recognition as an efficient technique to analyze polyolefin blends quantitatively, as it is considered to be superior to the conventional DSC method. It is quite certain that its use for blend analysis will become more common in the near future.

Cocrystallization is one of the limitations in Crystaf analysis. It seems that Tref is more appropriate for analyzing copolymers with complex CCD, especially if one needs more quantitative results. This is due to the fact that Tref analysis seems to be less affected by cocrystallization for the same CR. The fact that Tref also measures the differential profile directly, without the use of curve fitting and differentiation required in Crystaf, is responsible for the fact that Tref profiles generally appear sharper and more resolved than the equivalent Crystaf ones.

Although various mathematical models have been proposed recently to describe Crystaf and Tref, none can account for important phenomena such as crystallization kinetics and cocrystallization effects during the fractionation. From an academic viewpoint, the understanding of the fractionation mechanism operative in both techniques and the development of good phenomenological models is still a challenging task.

In conclusion, it can be said that both techniques are complementary in nature and will be used side by side for the better understanding of semicrystalline copolymers, combining the faster and easier use of Crystaf with the sharper resolution of Tref.

References

1. Monrabal BJ (1994) Appl Polym Sci 52:491
2. Monrabal B (1996) Macromol Symp 110:81
3. Cady LD (1987) Plast Eng 25
4. Gownder MJ (2001) Plast Film Sheeting 17:53
5. Soares JBP, Hamielec AE (1999) Temperature rising elution fractionation. In: Pethrick RA, Dawkins JV (eds) Modern techniques for polymer characterization. Wiley, New York, pp 15–55
6. Wild L (1990) Adv Polym Sci 98:1
7. Wild L, Blatz C (1993) Development of high performance tref for polyolefin analysis. In: Chung TC (ed) New advances in polyolefins. Plenum, New York, pp 147–157
8. Soares JBP, Hamielec AE (1995) Polymer 36:1639
9. Fonseca CA, Harrison IR (1999) Temperature rising elution fractionation. In: Pethrick RA, Dawkins JV (eds) Modern techniques for polymer characterization. Wiley, New York, pp 1–14
10. Flory PJ (1949) J Chem Phys 17:223
11. Flory PJ (1953) Principles of polymer chemistry, 1st edn. Cornell University Press, Ithaca, p 495
12. Mandelkern L (2002) Crystallization of polymers, 2nd edn. Cambridge University Press, Cambridge, p 90
13. Prasad A, Mandelkern L (1989) Macromolecules 22:4666
14. Nieto J, Oswald T, Blanco F, Soares JBP, Monrabal B (2001) J Polym Sci Part B Polym Phys 39:1616
15. Mandelkern L (2002) Crystallization of polymers, 2nd edn. Cambridge University Press, Cambridge, p 224
16. Stockmayer WH (1945) J Chem Phys 13:199
17. Simha R, Branson H (1944) J Chem Phys 12:253
18. Stejskal J, Kratochvil P, Strakova D (1981) Macromolecules 14:150
19. Stejskal J, Kratochvil P, Jenkins AD (1987) Macromolecules 20:181
20. Stejskal J, Kratochvil P (1987) Macromolecules 20:2624
21. Tacx JCJF, Linssen HN, German AL (1988) J Polym Sci Part B Polym Chem 26:61
22. Soares JBP, Hamielec AE (1995) Macromol Theory Simul 4:305
23. Costeux S, Anantawaraskul S, Wood-Adams PM, Soares JBP (2002) Macromol Theory Simul 11:326
24. Wild L, Ryle D, Knobeloch D, I Peat (1982) J Polym Sci Part B Polym Phys 20:441

25. Wild L, Ryle T (1977) Polym Prepr Am Chem Soc 18:182
26. Shirayama K, Kita S-I, Watabe H (1972) Makromol Chem 151:97
27. Burfield DR, Kashiwa N (1985) Makromol Chem 186:2657
28. Savitski EP, Caflisch GB, Killian CM, Meadows M, Merkley JH, Huff BJ (2003) J Appl Polym Sci 90:722
29. Anantawaraskul S, Soares JBP, Wood-Adams PM (2003) J Polym Sci Part B Polym Phys 41:1762
30. Kelusky EC, Elston CT, Murray R (1987) Polym Eng Sci 27:1562
31. Glockner GJ (1990) J Appl Polym Sci Appl Polym Symp 45:1
32. Pigeon M, Rudin A (1993) J Appl Polym Sci 47:685
33. Pigeon M, Rudin A (1994) J Appl Polym Sci 51:303
34. Usami T, Gotah Y, Takayama S (1986) Macromolecules 19:2722
35. Pasch H (2000) Adv Polym Sci 150:1
36. Springer H, Hengse A, Hinrichsen G (1990) J Appl Polym Sci 40:2173
37. Mirabella FM, Ford EA (1987) J Polym Sci Part B Polym Phys 25:777
38. Mingozzi I, Nascetti S (1996) Int J Polym Anal Character 3:59
39. Nakano S, Goto Y (1981) J Appl Polym Sci 26:4217
40. Zhou XQ, Hay JN (1993) Eur Polym J 29:291
41. Schouterden P, Groeninckx G, Van der Heijden B, Jansen F (1987) Polymer 28:2099
42. Hosoda S (1988) Polym J 20:383
43. Soares JBP, Abbott RF, Willis JN, Liu X (1996) Macromol Chem Phys 197:3383
44. Faldi A, Soares JBP (2001) Polymer 42:3057
45. Kim Y-M, Kim C-H, Park J-K, Kim J-W, Kim T-I (1996) J Appl Polym Sci 60:2469
46. Zhang M, Lynch DT, Wanke SE (2000) J Appl Polym Sci 75:960
47. Soares JBP, Hamielec AE (1995) Polymer 11:2257
48. Soares JBP (1998) Polym React Eng 199:1917
49. da Silva Filho AA, Soares JBP, de Galland GB (2000) Macromol Chem Phys 201:1226
50. Defoor F, Groeninckx G, Schanterden P, Van der Heijden B (1992) Polymer 33:3878
51. Borrajo J, Cordon C, Carella JM, Toso S, Goizueta G (1995) J Polym Sci Part B Polym Phys 33:1627
52. Elicabe G, Carella J, Borrajo J (1996) J Polym Sci Part B Polym Phys 34:527
53. Elicabe G, Cordon C, Carella J (1996) J Polym Sci Part B Polym Phys 34:1147
54. Britto LJD, Soares JBP, Penlidis A, Monrabal B (1999) J Polym Sci Part B Polym Phys 37:539
55. Pasch H, Brull R, Wahner U, Monrabal B (2000) Macromol Mater Eng 279:46
56. Gabriel C, Lilge D (2001) Polymer 42:297
57. Anantawaraskul S, Soares JBP, Wood-Adams PM, Monrabal B (2003) Polymer 44:2393
58. Sarzotti DM, Soares JBP, Penlidis A (2000) J Polym Sci Part B Polym Phys 40:2595
59. Brull R, Pasch H, Raubenheimer HG, Sanderson R, van Reenen AJ, Wahner UM (2001) Macromol Chem Phys 202:1281
60. Graef SM, Brull R, Pasch H, Wahner UM (2003) e-Polymers, no 05
61. Alamo RG, Viers BD, Mandelkern L (1993) Macromolecules 26:5740
62. Alamo RG, Domszy RC, Mandelkern L (1991) Macromolecules 24:6480
63. Richardson MJ, Flory PJ, Jackson JB (1963) Polymer 4:221
64. Shida M, Ficker HK, Stone IC (1966) J Polym Sci Polym Lett 4:346
65. Pasch H (2001) Macromol Symp 165:91
66. Brull R, Grumel V, Pasch H, Raubenheimer HG, Sanderson R, Wahmer UM (2002) Macromol Symp 178:81
67. Anantawaraskul S, Soares JBP, Wood-Adams PM (2004) Macromol Chem Phys 205:771

68. Monrabal B, Blanco J, Nieto N, Soares JBP (1999) J Polym Sci Part A Polym Chem 37:89
69. Simon LC, de Souza RF, Soares JBP, Mauler RS (2001) Polymer 42:4885
70. Soares JBP, Abbott RF, Kim JD (2000) J Polym Sci Part B Polym Phys 38:1267
71. Chu KJ, Shan CLP, Soares JBP, Penlidis A (1999) Macromol Chem Phys 200:2372
72. Chu KJ, Soares JBP, Penlidis A, Ihm SK (1999) Macromol Chem Phys 200:1298
73. Kim JD, Soares JBP (1999) Macromol Rapid Commun 20:347
74. Chu KJ, Soares JBP, Penlidis A (2000) Macromol Chem Phys 201:340
75. Kim JD, Soares JBP (2000) J Polym Sci Part A Polym Chem 38:1427
76. Shan CLP, Chu KJ, Soares JBP, Penlidis A (2000) Macromol Chem Phys 201:2195
77. Simon LC, Patel H, Soares JBP, de Souza RF (2001) Macromol Chem Phys 202:3237
78. Shan CLP, Soares JBP, Penlidis A (2002) J Polym Sci Part A Polym Chem 40:4426
79. de Goede S, Brull R, Pasch H, Marshall N (2003) Macromol Symp 193:35
80. Soares JBP, Monrabal B, Nieto J, Blanco J (1998) Macromol Chem Phys 199:1917
81. Beigzadeh D, Soares JBP, Duever TA (2001) J Appl Polym Sci 80:2200
82. Cheng HN, Tam SB, Kasehagen LJ (1992) Macromolecules 25:3779
83. Cheng HN, Kasehagen LJ (1993) Macromolecules 26:4774

Editor: Akihiro Abe